J. Fluid Mech. (2000), *vol.* 420, *pp.* 225–257. Printed in the United Kingdom

Miscible rectilinear displacements with gravity override. Part 1. Homogeneous porous medium

By MICHAEL RUITH AND ECKART MEIBURG†

Department of Aerospace and Mechanical Engineering, University of Southern California, Los Angeles, CA 90089-1191, USA

(Received 7 January 2000 and in revised form 16 May 2000)

Rectilinear homogeneous miscible displacements with gravity override are analysed by means of direct numerical simulations on the basis of the vorticity–streamfunction formulation of the governing equations. The vorticity-based point of view offers the advantage of clearly attributing the dominant flow characteristics to the effects of viscosity contrast, density difference, impermeable boundary conditions, or interactions among the above. Basic considerations regarding the vorticity field show that in an integral sense the coupling between viscosity and gravity vorticity is predominantly one way in nature, in that the gravity vorticity can amplify the viscous vorticity, but not vice versa. In particular, the vorticity point of view provides an explanation for the formation of the gravity tongue in terms of a focusing mechanism, which results from the combined action of the unfavourable viscosity gradient and the potential flow field generated by the interaction of the gravitational vorticity with the horizontal boundaries. This potential velocity field locally enhances the uniform global displacement velocity near the upper boundary, and thereby amplifies the viscous fingering instability along this section of the interface. In some parameter ranges, the gravity tongue exhibits interesting interactions with the viscous fingers next to it, such as pinching and partial merging. The influence of the Péclet number, the viscosity and density contrasts, and the aspect ratio on the dynamic evolution of the displacement is investigated quantitatively.

1. Introduction

The exploration of porous media flows involving fluids of different viscosities and/or densities has covered several decades. Early and relatively simple theoretical models for gravity-dominated flows were developed by Dietz (1953), cf. also the recent work by Yortsos (1991), and subsequently extended by Sheldon & Fayers (1962) as well as Fayers & Muggeridge (1990). These models are reasonably successful in predicting the rate of propagation of the so-called gravity tongue that often develops when density effects dominate. At the other end of the spectrum, displacements governed by viscosity effects have been investigated extensively as well, experimentally, theoretically, and by means of computations, dating back to the pioneering work of Hill (1952). In particular, the linear instability of the front responsible for the formation of viscous fingers has been analysed, along with their nonlinear growth

† To whom correspondence should be addressed, present address: Department of Mechanical and Environmental Engineering, University of California, Santa Barbara, CA 93110, USA, e-mail: meiburg@engineering.ucsb.edu

and interactions among them. Recent reviews of the field are given by Homsy (1987), Yortsos (1990), as well as McCloud & Maher (1995).

The intermediate regime, in which the competing gravitational and viscous forces approximately balance each other, represents an interesting parameter range whose dynamics are still only partially understood at this time. Depending on a variety of circumstances, such flows may or may not give rise to a gravity tongue, and to additional viscous fingers. Limited and somewhat qualitative information can be gained from the early two-dimensional experiments, performed in thin slabs, of Blackwell, Rayne & Terry (1959), van der Poel (1962), Pozzi & Blackwell (1963), as well as Crane, Kendall & Gardner (1963). More recently, novel experimental approaches have allowed three-dimensional investigations as well, cf. the computed tomography study of a quarter five-spot displacement by Withjack & Akervoll (1988). In addition, over the last decade or so large-scale numerical simulations have emerged as a useful new tool, which often can provide access to information that is difficult to extract experimentally. For example, Christie, Jones & Muggeridge (1990), Christie, Muggeridge & Barley (1993), as well as Sorbie, Zhang & Tsibuklis (1995) have been able to demonstrate good agreement between experiments and numerical simulations, which typically were based on conventional finite difference approaches. More recently, several experimental and computational investigations (Moisses, Miller & Wheeler 1989; Chang *et al.* 1991; Gorell 1992; Sorbie *et al.* 1992; Waggoner, Castillo & Lake 1992; Bacri *et al.* 1992; Araktingi & Orr 1993; Tchelepi *et al.* 1993; Lenormand 1995; Batycky, Blunt & Thiele 1996) have analysed the role of permeability heterogeneities in viscously unstable displacements.

While all of the above investigations clearly demonstrate that heterogeneity can significantly alter the dynamics of such displacements, the parameter regime in which viscosity, gravity and permeability effects are of comparable strength was addressed in detail only by the groups around Tchelepi, Orr and Salin. In particular, the detailed numerical work by Tchelepi (1994) was able to break new ground in this regard. This author employs a mixed computational approach that combines a traditional Eulerian finite difference discretization for the pressure equation with Lagrangian particle tracking for the concentration equation, in order to analyse the transition from viscosity- to density-dominated displacements, in both homogeneous as well as heterogeneous media, and furthermore in two as well as three dimensions. Comparisons indicate that if gravitational forces strongly dominate viscous forces, two- and three-dimensional simulations display similar behaviour. On the other hand, in the transitional region where buoyancy and viscous forces are of similar magnitude, significant discrepancies are observed, which can show the two-dimensional flow dominated by viscous fingering, while the three-dimensional displacement exhibits a strong influence of buoyancy forces.

Tchelepi furthermore presents a scaling analysis of the convective effects, i.e. in the absence of diffusion or dispersion. By normalizing the distance along each coordinate direction with the domain dimension in that direction, he is able to derive the relevant convective scaling groups that allow for comparisons between domains of different aspect ratios. In this way, he clearly identifies the role of the aspect ratio in determining the influence of gravitational segregation, which is shown to be more important in longer, thinner domains.

All of the above computational investigations employ formulations of the governing equations in primitive variables, i.e. velocity and pressure. While this approach may have the advantage that most researchers are familiar with analysing dynamical mechanisms in terms of these quantities, there are also some drawbacks. In particu-

lar, in this formulation the equations do not allow a clear separation of the various physical effects. Phrased differently, during the course of a numerical simulation it is difficult to distinguish which components of the pressure, or the velocity, are due to viscosity, or density, or permeability effects. In this regard, an alternative, vorticity-based formulation offers some clear advantages. Although it has been known at least since the work of de Josselin de Jong (1960) that the equations can be written in terms of the vorticity variable, the full potential of this approach has been realized only more recently, with the emergence of large-scale direct numerical simulations as a powerful tool for exploring the dynamics of porous media displacements. As will be discussed below, the equation governing the vorticity, and thereby the velocity, clearly identifies the components that are due to viscosity contrast, density difference, permeability variation and, in immiscible flows, surface tension. Hence the governing equations allow an interpretation of the displacement dynamics in terms of interactions among the different physical mechanisms, namely fingering instability, gravitational segregation, and channelling induced by heterogeneity fluctuations.

This possibility to interpret porous media flows in terms of their vorticity dynamics has been successfully exploited in the past, both for immiscible as well as miscible displacements. While Tryggvason & Aref (1983, 1985), Meiburg & Homsy (1988*a*, *b*) and others address the immiscible case, a number of more recent investigations focus on miscible flows. Tan & Homsy (1988) provide a vorticity-based explanation of the spreading, shielding and splitting sequence observed in neutrally buoyant, viscously unstable rectilinear displacements. Zimmerman & Homsy (1992) point to the absence of a vortex stretching term in the vorticity form of Darcy's law as the reason for the strong similarity between two- and three-dimensional porous media displacements, as opposed to Navier–Stokes flows. Tan & Homsy (1992) investigate heterogeneous rectilinear displacements. By interpreting the dynamical evolution of the flow in terms of the interacting viscosity- and permeability-related vorticity components, they are able to identify a resonance mechanism that occurs when these two components are active at comparable length scales. For quarter five-spot displacements, Chen & Meiburg (1998*b*) demonstrate that this resonance mechanism is responsible for the minimum in the breakthrough recovery observed at intermediate correlation lengths of the heterogeneity field. For a further analysis of the interaction of those two vorticity components, see de Wit & Homsy (1997*a*, *b*).

Manickam & Homsy (1995) treat the case in which gravity acts either parallel or antiparallel to the flow direction. Rogerson & Meiburg (1993*a*, *b*) focus on the mutual interaction of the viscosity- and gravity-related vorticity components in unbounded homogeneous displacements where gravity acts in the direction perpendicular to the flow. In their linear stability analysis, they identify the emergence of a quadrupole structure in the vorticity field as the main reason for the stabilization of the flow by gravitational forces. For non-monotonic viscosity profiles, similar observations of quadrupole structures in the vorticity field were made by Manickam & Homsy (1993, 1994) for rectilinear flows, as well as by Pankiewitz & Meiburg (1999) for the quarter five-spot configuration. As a final comment, it should be pointed out that the vorticity-based approach can aid in understanding other extensions as well, such as the influence of chemical reactions (de Wit & Homsy 1999).

The mutual interactions among all three of the vorticity contributions mentioned, i.e. viscosity, gravity and permeability components, to our knowledge have not yet been explored. Their analysis will be at the heart of the present investigation. In addition, we will focus on the interaction among these components in a finite rectilinear domain. As will be seen below, the boundary conditions that need to be satisfied as a result

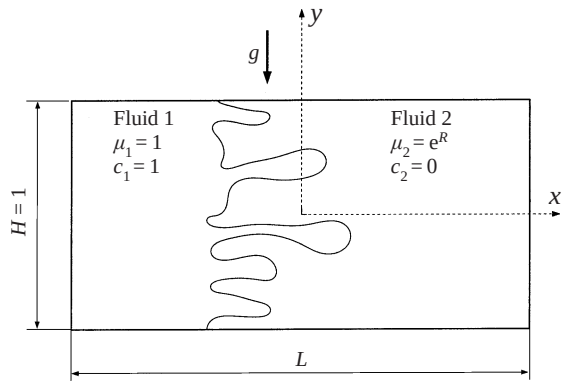

FIGURE 1. Principal sketch. An injected fluid 1 displaces a resident fluid 2 of different viscosity and density in a rectangular domain of height H and length L. Gravity points in the negative y-direction.

of the finite vertical extent of the flow domain give rise to an additional potential velocity field that can modify the interaction mechanisms among the different vorticity components. In order to establish and analyse the role of this potential velocity field, here (in part 1) we will address two-dimensional diplacements with viscosity and density contrasts in homogeneous, rectlinear domains. By comparing with the findings of Rogerson & Meiburg (1993*a*, *b*) for the infinite domain, we can thus evaluate the changes caused by the potential velocity component. Subsequently, part 2 (Camhi, Meiburg & Ruith 2000) extends the scope of the analysis by also including the effects of the permeability vorticity component. In particular, we will address such questions as whether or not the resonance mechanism observed in neutrally buoyant flows maintains its importance in the presence of density differences. It should be emphasized, however, that the goal of the present work lies not merely in the presentation of new computational results, but also in the development of a new perspective from which to interpret earlier numerical findings, in particular those by Tchelepi (1994). Consequently, this paper is organized as follows: In § 2, the governing equations, and boundary and initial conditions will be presented and recast into the vorticity–streamfunction formulation, and the relevant dimensionless parameters will be identified. Section 3 will give a brief description of the numerical technique, while § 4 will focus on the computational results and their interpretation in terms of the dynamically interacting vorticity components. Section 5 will provide additional discussion and comparisons.

2. Governing equations

We focus on the time-dependent evolution of incompressible miscible displacements in a rectangular domain such as depicted in figure 1. Assuming that the flow is governed by Darcy's law, the dimensional governing equations in the presence of density differences take the form

$$\nabla \cdot \boldsymbol{u} = 0, \tag{2.1a}$$

$$\nabla p = -\frac{\mu}{k}\boldsymbol{u} - \rho g \nabla y, \tag{2.1b}$$

$$\frac{\partial c}{\partial t} + \boldsymbol{u} \cdot \nabla c = D\nabla^2 c. \tag{2.1c}$$

Here, $\boldsymbol{u}$ denotes the velocity, p the pressure, and c the concentration of the displacing fluid. Viscosity and density are indicated by μ and ρ, respectively, while k represents the permeability of the porous medium. The gravitational acceleration of magnitude g is assumed to point in the negative y-direction. The above set of equations, which also served as the basis for the earlier investigations by Rogerson & Meiburg (1993*a*, *b*), express the conservation of mass, momentum, and species. As a first step in the computational investigation, only molecular diffusion is accounted for, as expressed by a scalar diffusion coefficient D. This represents a relatively crude approximation of the real diffusion and dispersion mechanisms acting at a dynamically evolving miscible interface inside a porous medium. First of all, even in the absence of any motion the dependence of the scalar diffusion coefficient on the concentration can strongly affect the nature of the concentration field (Petitjeans & Maxworthy 1996; Chen & Meiburg 1996). Furthermore, the effects of flow-induced dispersion (Taylor 1953; Horne & Rodriguez 1983) are typically significant in a porous environment, cf. the overview given by Brady & Koch (1988). Attempts have been made to account for such effects by replacing D with a dispersion tensor (Yortsos & Zeybek 1988; Zimmerman & Homsy 1991; Zhang, Sorbie & Tsibuklis 1997) based on a Taylor-type model. However, there are indications that this approach still suffers from some shortcomings, cf. the comparisons between experiments and simulations performed by Petitjeans *et al.* (1999) in a Hele-Shaw cell. Since at present there are no dispersion models available that can properly account for the evolution of miscible flows even in simple geometries (Petitjeans & Maxworthy 1996; Chen & Meiburg 1996; Yang & Yortsos 1997; Rakotomalala, Salin & Watzky 1997), we feel that it is best to employ a scalar diffusion coefficient for now, in order not to obscure the identifiable physical mechanisms at work.

Both the viscosity and the density are supposed to be known functions of the concentration, and the permeability k has a given spatial distribution

$$\mu = \mu(c), \quad \rho = \rho(c), \quad k = k(x, y). \tag{2.2}$$

The point permeability is assumed to be isotropic, i.e. k is taken to be a scalar. For the remainder of this paper, we will furthermore limit ourselves to two-dimensional homogeneous displacements, so that $k = K = \text{const}$. The two-dimensional case in which k varies as a function of location will be treated in part 2.

2.1. *Scaling considerations*

In order to render the governing equations dimensionless, characteristic scales have to be introduced. A detailed and lucid analysis of the pertinent scaling considerations for displacements in a domain of finite length L and height H is provided by Tchelepi (1994). In particular, he points out that in the absence of dispersive and diffusive effects, scaling of the spatial coordinates (x, y) with the respective dimensions (L, H) of the flow domain (convective scaling) allows similarity considerations among reservoirs of different aspect ratios

$$A = \frac{H}{L}. \tag{2.3}$$

In the presence of diffusive/dispersive effects, however, this similarity cannot be maintained by either convective or dispersive scaling. Consequently, in order to render the governing equations dimensionless for the present problem, we take the vertical extent H of the flow domain as the characteristic length scale in both directions. The nominal displacement velocity U serves as the velocity scale, so that a time scale is obtained as H/U. By furthermore scaling viscosity, density, and pressure with μ_1,

$\rho_2 - \rho_1$, and $\mu_1 UH/K$, respectively, where the subscript 1 indicates the displacing fluid, we obtain the dimensionless form of the governing equations as

$$\nabla \cdot \boldsymbol{u} = 0, \tag{2.4a}$$

$$\nabla p = -\mu \boldsymbol{u} - G\rho \nabla y, \tag{2.4b}$$

$$\frac{\partial c}{\partial t} + \boldsymbol{u} \cdot \nabla c = \frac{1}{Pe} \nabla^2 c, \tag{2.4c}$$

where the Péclet number

$$Pe = \frac{UH}{D} \tag{2.5}$$

can be interpreted as a dimensionless flow rate, and the gravity parameter G has the form

$$G = \frac{g\,(\rho_2 - \rho_1)\,K}{U\mu_1}. \tag{2.6}$$

It should be pointed out that other, slightly different definitions of gravity parameters have been used in the literature, e.g. Fayers & Muggeridge (1990). Note that in the above definition, as a result of using H as the characteristic length scale in both the x- and y-directions, our definition of the dimensionless parameter that expresses the relative importance of viscous and gravitational forces differs from the one derived by Tchelepi (1994) for flows without diffusion and/or dispersion. In addition, he uses the viscosity difference as the characteristic viscosity, rather than the viscosity of the injected fluid. Apart from this minor difference, the so-called viscous-to-gravity ratio J derived by the convective scaling arguments, is related to G as

$$J \sim \frac{A}{G}. \tag{2.7}$$

By defining the rise velocity of the injected fluid as

$$V = kg\frac{\Delta\rho}{\Delta\mu}, \tag{2.8}$$

Tchelepi then interprets J as the ratio of two time scales, t_g and t_v, respectively

$$J = \frac{t_g}{t_v}, \tag{2.9}$$

where t_g indicates the time it takes the lighter, injected fluid to rise by a distance equal to the height of the domain, and t_v denotes the time necessary for the mean displacement to reach the outlet. This scaling argument demonstrates that, under convective transport only, the aspect ratio of the domain needs to be included when assessing the relative importance of viscous and gravitational forces, in order to properly account for gravity segregation effects. It thus becomes obvious that these are more dominant in longer and thinner domains, where the lighter fluid has more time to rise to the top. One of the goals of the present investigation is to evaluate the applicability of these convective scaling arguments in the presence of small, but non-negligible, amounts of diffusion.

Following other researchers (e.g. Tan & Homsy 1988; Rogerson & Meiburg 1993*a*, *b*; Chen & Meiburg 1998*a*, *b*), we define

$$R = -\frac{1}{\mu}\frac{\mathrm{d}\mu}{\mathrm{d}c} \tag{2.10}$$

and consider R to be a constant for a given combination of fluids. In this way, the

viscosity dependence on the concentration has the form

$$\mu(c) = \mathrm{e}^{R(1-c)}\,. \tag{2.11}$$

Alternatively, other viscosity–concentration relationships, such the quarter-power blending rule (e.g. Tchelepi 1994 and references therein), could easily be implemented as well. Furthermore, we assume a linear relationship between density and concentration, so that we can write

$$\rho = \frac{\rho_2}{\rho_1 - \rho_2} + c. \tag{2.12}$$

By absorbing the constant term in the density–concentration relationship into the pressure, Darcy's law thus reduces to

$$\nabla p = -\mu \boldsymbol{u} - Gc\nabla y. \tag{2.13}$$

As discussed above, it is instructive to recast the governing equations into a vorticity (ω) and streamfunction (ψ) formulation (de Josselin de Jong 1960). Here ψ accounts only for deviations of the fluid motion from the constant base flow, so that we obtain

$$\omega = \frac{\partial v}{\partial x} - \frac{\partial u}{\partial y}, \quad u = 1 + \frac{\partial \psi}{\partial y}, \quad v = -\frac{\partial \psi}{\partial x}. \tag{2.14a–c}$$

It follows that streamfunction and vorticity are related by the Poisson equation

$$\nabla^2 \psi = -\omega. \tag{2.15}$$

By taking the curl of Darcy's law, we furthermore obtain

$$\omega = -R\nabla\psi \cdot \nabla c + \frac{G}{\mu} c_x. \tag{2.16}$$

This equation demonstrates the existence of two vorticity modes, related to viscosity and density, respectively. Rogerson & Meiburg (1993*a*, *b*) investigated the linear and nonlinear interaction of these two modes in an infinite, doubly periodic domain, i.e. in the presence of a uniform potential velocity component only. In contrast, the finite domain considered in the present work will give rise to a spatially and temporally evolving, non-uniform potential velocity component, by way of the set of conditions that need to be satisfied along the boundaries of the finite domain, cf. the analysis below. This potential velocity component will interact with each of the vortical modes, and thereby it will affect their mutual interaction as well.

Boundary conditions are prescribed as follows:

$$x = \pm 0.5/A\text{:} \quad \psi_x = 0, \quad \omega_x = 0, \quad c_x = 0, \tag{2.17a}$$

$$y = \pm 0.5\text{:} \quad \psi = 0, \quad c_y = 0. \tag{2.17b}$$

They determine the overall volume flux through the inflow and outflow boundaries and set the vertical velocity at these boundaries to zero, while allowing the horizontal velocity $u(y)$ to adjust itself. Alternatively, the condition $\psi = 0$ could be imposed at the inflow and outflow boundaries, which would correspond to setting the horizontal velocity component equal to the nominal displacement velocity. For a more detailed discussion of the relative merits of these boundary conditions, see Tchelepi (1994). Furthermore, the mass flux across the horizontal boundaries vanishes. Initial conditions are specified as

$$\psi(\boldsymbol{x}, t = 0) = \omega(\boldsymbol{x}, t = 0) = 0, \tag{2.18a}$$

$$c(\boldsymbol{x}, t=0) = 0.5\left\{1 - \mathrm{erf}\left[\left(x + 0.5/A - \frac{4}{\sqrt{Pe}}\right)\sqrt{Pe}\right]\right\}. \tag{2.18b}$$

In this way, a singular initial condition for the concentration at the inflow boundary is avoided, and instead a continuous concentration profile is prescribed that decreases from $c \approx 1$ at the inflow to $c \approx 0$ over a distance of $O(Pe^{-1/2})$. The profile initially is centred a small distance $4Pe^{-1/2}$ away from the inflow boundary. Perturbations are imposed at $t = 0$ by randomly varying this thickness of the initial concentration profile as a function of the vertical coordinate.

3. Numerical technique

In principle, the problem at hand does not have any intrinsic symmetries that allow the application of Fourier methods. However, the boundary conditions of vanishing x-derivatives for streamfunction, vorticity and concentration at $x = \pm 0.5/A$ enable us to employ a Galerkin-type discretization using cosine expansions for these variables in the streamwise direction:

$$\psi(x, y, t) = \sum_k \hat{\psi}_k(y, t)\, \cos\left[k\,\alpha\,(x + 0.5/A)\right], \tag{3.1a}$$

$$\omega(x, y, t) = \sum_k \hat{\omega}_k(y, t)\, \cos\left[k\,\alpha\,(x + 0.5/A)\right], \tag{3.1b}$$

$$c(x, y, t) = \sum_k \hat{c}_k(y, t)\, \cos\left[k\,\alpha\,(x + 0.5/A)\right], \tag{3.1c}$$

with

$$|k| < \frac{N_1}{2}, \quad \alpha = 2\pi A, \tag{3.2}$$

where N_1 is the number of grid points in the longitudinal direction. This type of Fourier–Galerkin scheme is very attractive to use in the present context, since it allows a fast and efficient solution of the Poisson equation for the streamfunction. The time integration is fully explicit and utilizes a third-order Runge–Kutta procedure (Wray 1991), so that by writing the concentration equation as

$$\frac{\partial c}{\partial t} = F(c), \tag{3.3}$$

we obtain

$$c_{i,j}^k = c_{i,j}^{k-1} + \Delta t\left[\gamma_k F\left(c_{i,j}^{k-1}\right) + \eta_k F\left(c_{i,j}^{k-2}\right)\right], \tag{3.4}$$

where

$$\gamma_1 = \tfrac{8}{15}, \quad \eta_1 = 0, \tag{3.5a}$$

$$\gamma_2 = \tfrac{5}{12}, \quad \eta_1 = -17/60, \tag{3.5b}$$

$$\gamma_3 = \tfrac{3}{4}, \quad \eta_1 = -5/12. \tag{3.5c}$$

The evaluation of the nonlinearity at each time level is performed in a pseudo-spectral manner (cf. Canuto *et al.* 1988). This involves a forward Fourier transform of the velocity components and the vorticity, the computation of the nonlinear products in real space and the backward transform of the products to wavenumber space. For the differentiation in the normal direction, we employ compact finite differences in the form given by Lele (1992), which are of sixth order in the interior of the flow domain. More details on the implementation of these schemes for miscible porous

media flows are provided by Meiburg & Chen (2000), Chen (1998), as well as Chen & Meiburg (1998*a*, *b*). It should be noted that, in contrast to many schemes based on the velocity and pressure variables, the mass conservation properties are not a concern for the present approach, since the formulation of the governing equations in terms of vorticity and streamfunction satisfies the continuity equation identically. The time step is continuously adjusted so that it always satisfies both the CFL-condition, as well as the limitations caused by the diffusive terms. The simulations to be discussed below typically employ discretizations of 1024×512 grid points. The code was validated by comparing the growth rates of small perturbations with the respective values obtained from linear stability theory, in the absence of density differences. For a comparison between purely spectral and mixed spectral/compact finite difference simulations of a different class of flows, the reader is referred to Härtel, Meiburg & Necker (2000). The data presented there confirm that the mixed approach yields results of an accuracy that is comparable to the purely spectral approach.

4. Results

In the following, we will commence by describing the temporal and spatial evolution of a typical flow, which can subsequently serve as a reference case when discussing the effects of variations in the individual parameters. At first, the simulation results will serve to identify the dominant mechanisms in qualitative terms. Subsequently, several quantitative measures of the flow evolution will be introduced, and their dependence on the values of the governing parameters will be discussed.

4.1. *Reference case*

As representative reference case, a displacement is selected for which the dimensionless parameters have values of $Pe = 2000$, $G = 1$, $R = 3$, and $A = 0.5$. This value of Pe is near the upper limit of what can be resolved with the present grid. The other parameter values were chosen in order to demonstrate many of the mechanisms that govern displacements with density variations.

Figure 2 shows time sequences of the concentration fields for the reference case. Soon after the start of the simulation, numerous small fingers can be seen to develop. However, even though the flow remains predominantly horizontal, the comparatively thin finger at the top of the domain quickly outgrows all others and subsequently develops into a narrow gravity tongue that increasingly dominates the flow. It eventually results in the breakthrough of the flow at the early time of $t = 0.530$, however, not without undergoing some interesting and complex interactions with other fingers evolving in the flow. While the emergence of further viscous fingers, and their growth to large amplitudes, is not completely prevented, these fingers have barely reached the halfway point in the x-direction by the time of breakthrough. Nevertheless, they display an interesting dynamic behaviour of their own, involving several examples of spreading, shielding, and merging. Of particular interest is the interaction of the gravity tongue with the finger directly below it.

Around $t = 0.2$ this finger approaches the gravity tongue from below, thereby temporarily pinching it and reducing its supply of less-viscous fluid. This is reflected in a transient slowdown of the tip of the gravity tongue, cf. figure 3. In this process, the tip of the finger below the gravity tongue spreads laterally, and between $t = 0.2$ and 0.3 its upper part merges with the gravity tongue, while its lower part proceeds downward and away from the gravity tongue. This partial merger replenishes the fluid supply of the gravity tongue. However, around $t = 0.4$ and 0.5 additional pinchings

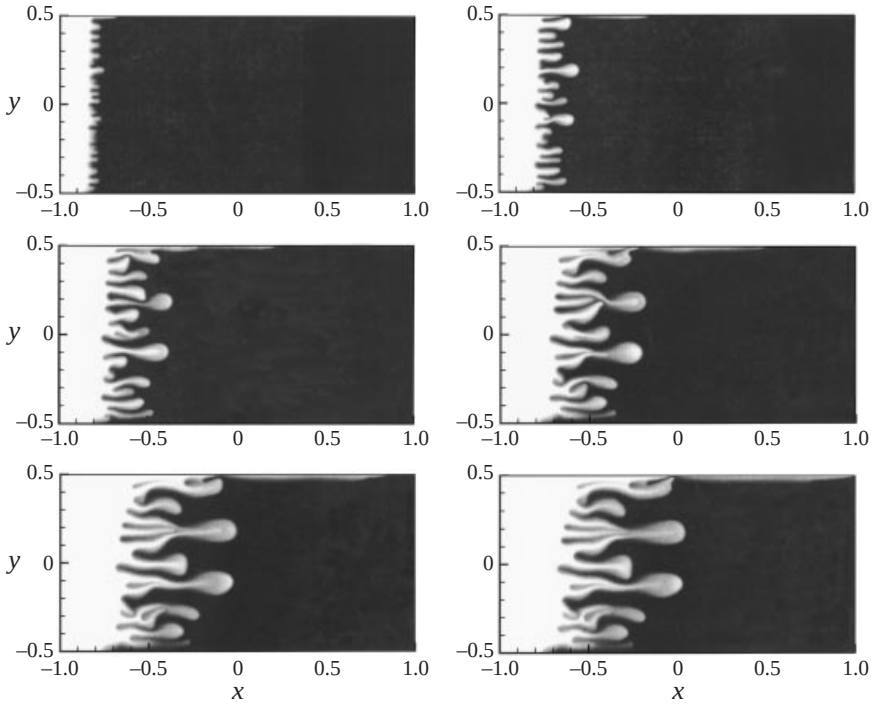

FIGURE 2. Reference case: $Pe = 2000$, $G = 1$, $R = 3$, and $A = 0.5$. Concentration field at times $t = 0.1$, 0.2, 0.3, 0.4, 0.5, and 0.530. In addition to numerous interacting fingers, a narrow gravity tongue evolves that results in an early breakthrough of the injected fluid.

and subsequent partial mergers can be observed, suggesting that these events occur repeatedly in an almost periodic fashion. Similar interactions between the gravity tongue and the finger immediately below it, involving pinching as well as partial or complete merging, were observed in the particle tracking simulations of Tchelepi (1994), as well as in the experiments and finite difference simulations of Christie *et al.* (1990). It is of interest to observe that the two dominant fingers in the central region of the domain proceed predominantly in the horizontal direction, with at most a very small upward velocity component. This indicates that for the present value of $G = 1$, the density differences are unable to generate strong vertical velocities in the mixing zone, i.e. the zone dominated by viscous fingering. Consequently, the bulk of the vertical fluid transport appears to occur in the unmixed regions ahead of and behind the fingering zone, rather than through fingers with substantial angles of inclination. This is also confirmed by the corresponding streamline patterns presented in figure 4, which indicate a moderate slope of the streamlines both upstream and downstream of the mixing zone. The contour plots for the two vorticity components at $t = 0.5$ (figure 5) indicate a layered structure inside the fingers due to the viscous component, along with a mushroom structure at the heads and tails of the dominant fingers, due to the gravitational component. With regard to the above observations, however, one has to keep in mind that the parameter values characterizing the transitional regime between gravity- and fingering-dominated flows change when three-dimensional effects are taken into account (Tchelepi 1994). Thus, there is a strong motivation to extend the current investigation to three dimensions.

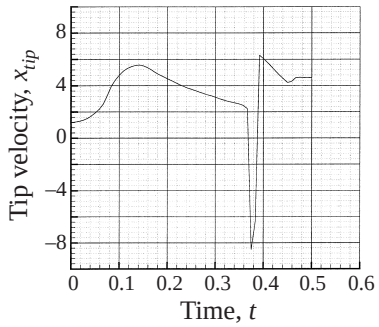

FIGURE 3. Reference case: tip velocity of the gravity tongue as a function of time. The periodic slowdown and speedup phases reflect the interaction of the gravity tongue with the finger immediately below it. The large negative spike around $t = 0.375$ reflects the fact that the concentration in the tip of the gravity tongue temporarily drops below the threshold value of 0.5, which serves to establish the tip location.

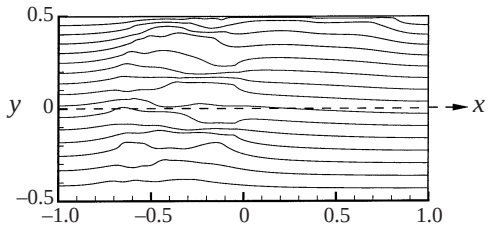

FIGURE 4. Reference case: streamfunction contours at time $t = 0.5$. The streamlines have a modest slope in the regions ahead of and behind the front, indicating that the bulk of the vertical fluid transport occurs outside the fingering zone.

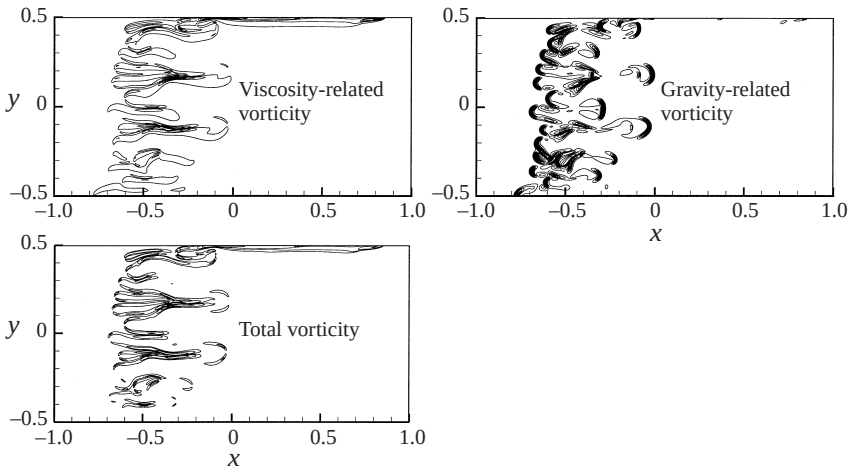

FIGURE 5. Reference case: vorticity contours at time $t = 0.5$. The layered structures along the length of the fingers, are due to the viscous vorticity component.

4.1.1. *Vorticity considerations*

In order to understand the mutual interaction between the evolving viscous fingers and the flow component induced by gravity, it is instructive to focus on the respective

vorticity components. When integrating the gravitational vorticity component

$$\omega_G = \frac{G}{\mu} c_x \tag{4.1}$$

over the entire flow domain S, it becomes clear immediately that due to the constant concentration values far ahead of and behind the front, the resulting gravitational circulation

$$\Gamma_G = \int_S \omega_G \, \mathrm{d}S = \frac{G}{Re^R} \int_S \frac{\partial}{\partial x} \left(\mathrm{e}^{Rc} \right) \mathrm{d}S = -\frac{G}{R} \left(1 - \mathrm{e}^{-R} \right) \tag{4.2}$$

is independent of time. Note that, by expanding e^{-R} into a power series, it is easily shown that for $R = 0$ one obtains $\Gamma_G = -G$. In a global sense, the tendency of the velocity field associated with the gravitational vorticity component to rotate or tilt the concentration field thus remains active at a roughly constant level for all times, independent of Pe and A. As a result, the accumulated effect of gravity on the concentration field, as expressed by a time integral over the gravitational vorticity component, will grow proportionally to time. For this reason, the effects of gravity should become increasingly obvious for longer times. The above line of reasoning is confirmed, for example, by the numerical observations of Tchelepi (1994), who points out the crucial role of the domain aspect ratio, i.e. of the overall displacement time, in determining the transition from fingering to gravity-dominated flow.

For the viscous vorticity component

$$\omega_v = R \left(-uc_y + vc_x \right) \tag{4.3}$$

a corresponding exact analytical integration cannot be performed. However, some qualitative insight can still be gained from approximate estimates. The viscous vorticity component is limited to those regions in which the concentration varies, i.e. along the miscible interface between the two fluids. Once the fingers have reached a significant amplitude, most of the interface will be oriented in the streamwise x-direction, so that the first term in equation (4.3) dominates. This term indicates that negative vorticity is located along those interfacial sections where the lighter, displacing fluid moves above the heavier, displaced fluid, and vice versa. In a neutrally buoyant displacement, there will be approximately equal lengths of interfacial segments with positive and negative vorticity, respectively, and as a result the viscous circulation

$$\Gamma_v = \int_S \omega_v \, \mathrm{d}S \tag{4.4}$$

will be close to zero. This will no longer hold if buoyancy effects are sufficiently strong to create a gravity tongue, such as in the reference flow discussed above. In such cases, as a result of the effects of the gravitational circulation, interfacial sections along which lighter fluid moves above heavier fluid will dominate, and consequently there will be more negative than positive viscous vorticity. In this way, the gravitational vorticity strengthens the viscous vorticity component that is of the same sign, while weakening the component of opposite sign.

This is clearly visible in figure 6, which separately shows the overall negative and positive circulation components in the flow field, along with their sum. The value of this sum initially is entirely due to the gravitational circulation. However, its subsequent growth reflects the effect described above of the gravitational vorticity on the respective viscous vorticity components. It thus provides us with a quantitative measure to diagnose whether or not gravitational effects are becoming dominant. In

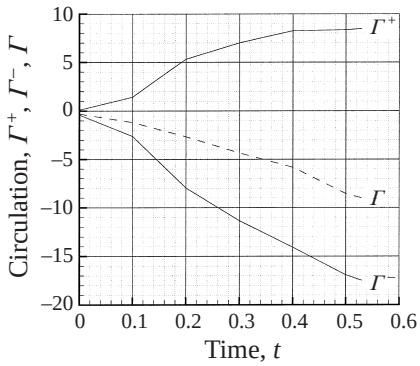

FIGURE 6. Reference case: the temporal evolution of the negative and positive circulation components in the flow field, as well as their sum. The initial value of this sum is entirely due to the gravitational circulation. The value of the gravitational circulation component remains constant for all times, so that the growth of the sum reflects the amplification (damping) of the negative (positive) component of the viscosity circulation by the gravitational component.

this context, it is furthermore important to point out that this interaction between the gravitational and viscous circulations is one-way in nature, as far as the overall gravitational circulation is concerned. In other words, while the gravitational circulation affects the magnitude of the respective viscous components, there is no reverse effect, since the magnitude of the gravitational circulation is constant and cannot be changed by the actions of the viscous circulation. However, the local distribution of the gravitational vorticity might of course very well be affected by the viscous vorticity component. The above considerations regarding the quantitative evolution of the vorticity field will have to be modified if the porous medium exhibits inhomogeneities, cf. the corresponding analysis in part 2. These inhomogeneities will result in a third contribution to the scalar vorticity, whose influence on and interaction with the above two components will be analysed in detail. Furthermore, these interactions become significantly more complicated in three-dimensional displacements, where the vorticity variable is a vector whose three components are governed by different respective interactions of the various physical mechanisms.

4.1.2. *Potential velocity field*

The emergence of a gravity tongue represents an important feature in many porous media flows dominated by gravity, as it can result in the early breakthrough of the displacing fluid. Interestingly, such a gravity tongue was not observed in the simulations by Rogerson & Meiburg (1993*b*), which were performed in a domain of infinite extent in both the horizontal and the vertical directions. In this context, it is important to appreciate that the dynamical evolution of the flow is governed not only by the interacting vorticity components, but also by their interplay with the potential velocity field. This potential velocity field, in turn, consists of the constant uniform base flow plus an additional time-dependent contribution that is generated by the horizontal boundaries in order to enforce the condition of vanishing normal flow. The role of this potential velocity component, which was absent in the simulations of Rogerson & Meiburg (1993*b*), will now be discussed. Consider the model situation in which the reservoir is infinite in the horizontal direction and extends from $y = -0.5$ to $y = 0.5$ in the vertical direction. Assume that the two fluids of different densities and viscosities are initially separated by a sharp vertical interface at $x = 0$. In the

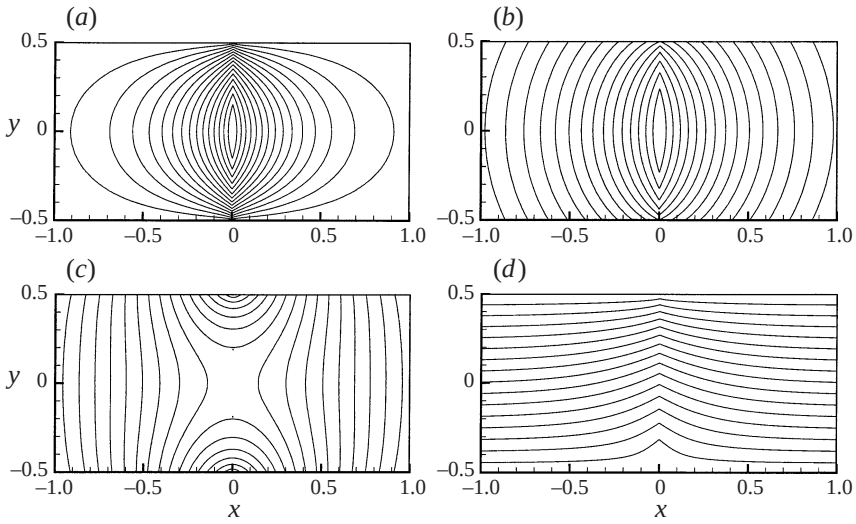

FIGURE 7. (*a*) Streamfunction due to a constant vertical vortex sheet located at $x = 0$ inside a horizontally infinite domain that extends from $y = -0.5$ to $y = 0.5$ in the vertical direction. (*b*) Streamfunction component due to the same vortex sheet in a vertically infinite domain. (*c*) Potential streamfunction component inside the vertically finite domain due to all of the image vortex sheets outside the domain, or equivalently, due to the presence of the horizontal boundaries. (*d*) Superposition of the streamfunction shown in (*a*) with a uniform net displacement in the x-direction.

absence of any net horizontal displacement, the pressure and velocity fields during the ensuing rotation of the interface were analysed by Verruijt (1980). From the governing equations, it follows immediately that the initial vorticity field corresponds to a constant-strength vortex sheet at $x = 0$

$$\omega_0(x, t = 0) = \Delta V\, \delta(0), \tag{4.5}$$

where ΔV is the vertical velocity jump across the interface caused by the density difference, and δ represents the Dirac delta function. C. Härtel (1997, personal communication) showed that this initial vorticity field results in the streamfunction

$$\psi(x, y, t = 0) = \frac{2\Delta V}{\pi^2} \sum_{k=0}^{\infty} \frac{(-1)^k}{(2k+1)^2} \mathrm{e}^{-(2k+1)\pi|x|} \cos\left[(2k+1)\,\pi y\right] \tag{4.6}$$

shown in figure 7(*a*).

As is well known from potential flow theory, for the present set of symmetry conditions at the top and bottom boundaries, which allow for slip but not for a normal velocity component, this streamfunction is the result of two contributions from the vorticity field: the constant-strength vortex sheet inside the domain (corresponding streamfunction shown in figure 7*b*), and all of the image vortex sheets above and below the domain needed to satisfy the symmetry conditions (related streamfunction depicted in figure 7*c*). The contribution of the image vortex sheets in effect takes the form of a potential flow field inside the domain, which can be attributed to the existence of the horizontal boundaries at $y = \pm 0.5$.

As can be seen in figure 7(*c*), for the present case of a uniform net displacement this potential velocity field adds a horizontal flow component to the average displacement velocity near the top of the domain. In the presence of an unfavourable viscosity contrast it effectively strengthens locally the unstable nature of the displacement

process and thereby encourages the formation of a dominant viscous finger at the top of the domain. This is also reflected by figure 7(*d*), which is obtained by superimposing the uniform net displacement in the x-direction on the flow shown in figure 7(*a*). Thus, we can attribute the emergence of the gravity tongue to the interaction of the potential velocity field generated by the boundaries with the unstable viscosity gradient. Hence the rapid growth of the gravity tongue is caused by the same principal interaction mechanism of a potential flow with an unstable viscosity gradient as the basic fingering instability. In a sense, the boundaries effectively 'focus' the effects of the unstable viscosity gradient and the density jump on a narrow region just below the top boundary. This focusing mechanism is clearly visible in figure 7(*d*). The important role of the viscosity contrast is also demonstrated by a comparison of the local flow features near the top and the bottom of the domain. In the absence of a viscosity contrast, i.e. for $R = 0$, these two flow regions would be symmetric to each other. The fact that no gravity tongue evolves near the bottom reflects the fact that there the potential flow component interacts with a stable viscosity gradient.

4.2. *Influence of gravity parameter G*

It is instructive to compare the above reference case to a simulation for $Pe = 2000$, $G = 0$, $R = 3$, and $A = 0.5$, with identical initial perturbations. Concentration plots are shown for different times in figure 8. Interestingly, up to the time when the case of $G = 1$ breaks through, the two flows are nearly identical to each other throughout the interior of the domain, with the only significant differences occurring near the top, where for $G = 1$ the gravity tongue emerged, and much smaller deviations near the very bottom of the fingering zone. This confirms that for $G = 1$, the combined effects of unfavourable viscosity contrast and density difference focused on a narrow layer near the top boundary, without significantly affecting the shape, direction, or dynamics of the dominant fingers in the central domain. Scaling results for the thickness of the gravity tongue produced in this narrow layer will be presented below. Instead, the gravitational forces effectively cause small vertical velocities throughout widespread regions of unmixed fluid covering the entire vertical extent of the reservoir. The vorticity contours also (figure 9) confirm that substantial differences between the two flows are limited to the regions near the top and bottom boundaries of the reservoir.

Two cases that fall in between the two flows discussed above are shown in figures 10 ($G = 0.25$) and 11 ($G = 0.5$), with all other parameters left unchanged. Together with the neutrally buoyant flow in figure 8 and the reference case in figure 2, these illustrate the gradual transition from a flow without density effects to one dominated by a gravity tongue. For the smaller value of the gravity parameter ($G = 0.25$), a weak finger is seen to emerge at the top of the reservoir. However, it fails to achieve a dominant role by the time of breakthrough. It seems possible that this finger would eventually develop into a full-scale gravity tongue if the reservoir were longer. Alternatively, the more advanced finger in the central domain might grow towards the top and eventually take over the role of a gravity tongue in a longer reservoir. This issue is resolved by a corresponding calculation for the aspect ratio $A = 0.25$, which indicates that the finger growing along the top of the reservoir indeed develops into a dominant gravity tongue, see figure 12.

The overall sum of the positive and negative circulation components for the different flows is depicted in figure 13. It can be seen that this overall circulation tends to grow with time for all values of G, as long as $G > 0$. This suggests that the continued amplification of the negative component of the viscosity-related vorticity by the gravitational circulation component will inevitably lead to the eventual emergence

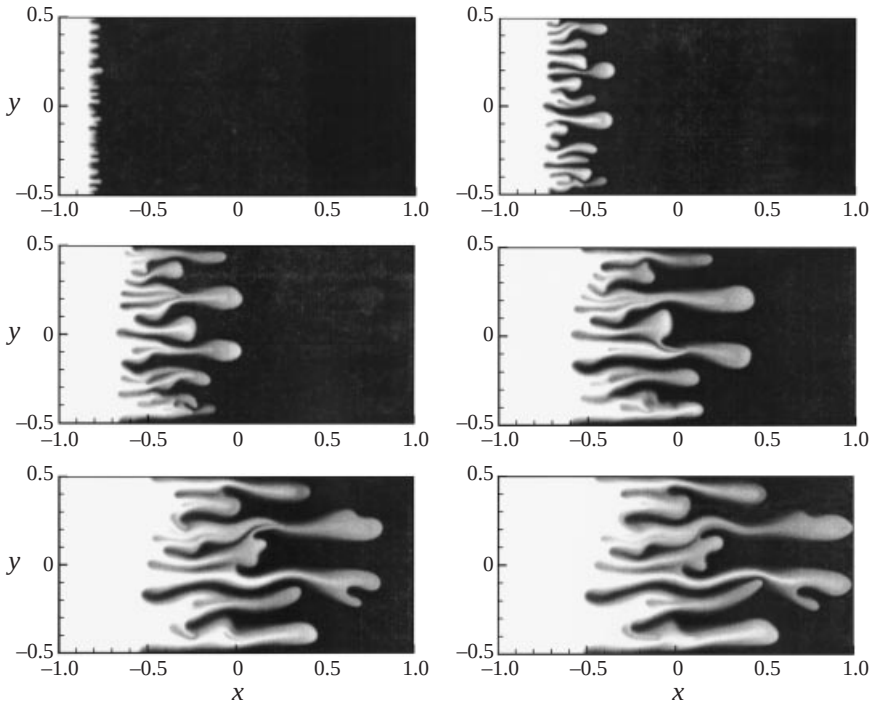

FIGURE 8. $Pe = 2000$, $G = 0$, $R = 3$, and $A = 0.5$: concentration field at times $t = 0.1$, 0.3, 0.5, 0.7, 0.9, and 0.984. In the interior of the domain, this neutrally buoyant flow develops nearly identically to the gravity-dominated reference case. This indicates that in the reference case, the effects of buoyancy are effectively limited to the narrow flow regions near the top and bottom of the domain.

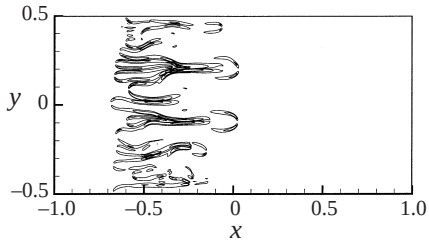

FIGURE 9. $Pe = 2000$, $G = 0$, $R = 3$, and $A = 0.5$: vorticity contours at time $t = 0.5$. Differences compared to the reference case are limited to narrow regions near the top and bottom of the flow domain.

of a gravity tongue, provided that a sufficient amount of time is available, i.e. that the domain is long enough. However, we also observe that, as long as no dominant gravity tongue has emerged yet, the circulations for the cases $G = 0.125, 0.25$, and 0.5 develop very similarly to each other, which reflects the fact that for these parameters significant differences in the concentration fields are limited to narrow regions near the top and bottom boundaries.

Regarding the transition from a neutrally buoyant flow dominated by viscosity effects to one characterized by a strong gravity tongue, it is furthermore interesting to note that by the time of breakthrough the case $G = 0.25$ (figure 10) displays more tip splittings than the case $G = 0$ (figure 8). While the number of splitting events in these

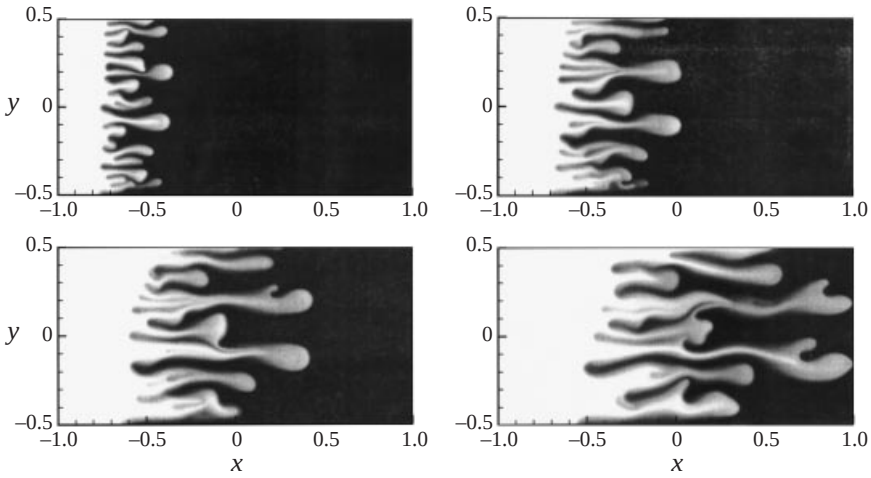

FIGURE 10. $Pe = 2000$, $G = 0.25$, $R = 3$, and $A = 0.5$: concentration field at times $t = 0.3$, 0.5, 0.7, and 0.984. At this weak level, gravitational effects do not result in the formation of a dominant gravity tongue by the time breakthrough occurs.

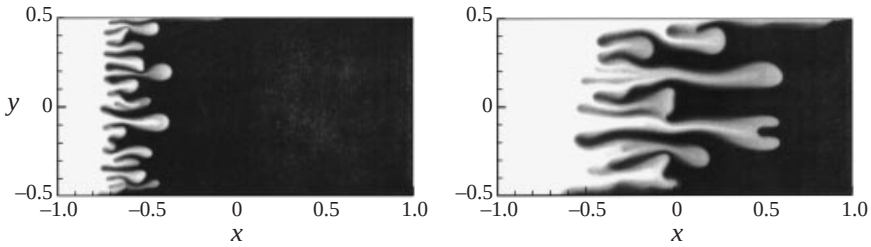

FIGURE 11. $Pe = 2000$, $G = 0.5$, $R = 3$, and $A = 0.5$: concentration field at times $t = 0.3$ and 0.815. Here a gravity tongue forms that results in an early breakthrough.

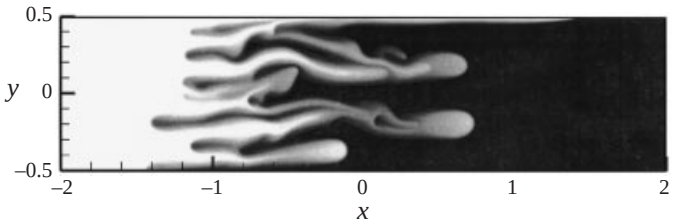

FIGURE 12. $Pe = 2000$, $G = 0.25$, $R = 3$, and $A = 0.25$: concentration field at time $t = 1.4$. This simulation indicates that in a longer domain, the finger growing along the top of the reservoir in figure 10 develops into a dominant gravity tongue.

flows is too small to be statistically significant, we did observe the same trend for other parameter combinations. We suspect that small amounts of cross-flow induced by moderate density differences are responsible for this tendency towards increased tip splitting. For large density differences, of course, both the fingering itself, as well as the tip splitting, becomes less prominent.

For $G = 2$ and $G = 4$, with all other parameters left unchanged, the cumulative effect of the distributed gravitational vorticity is substantially stronger, which in turn generates a larger potential velocity component as a result of the no-flux boundary

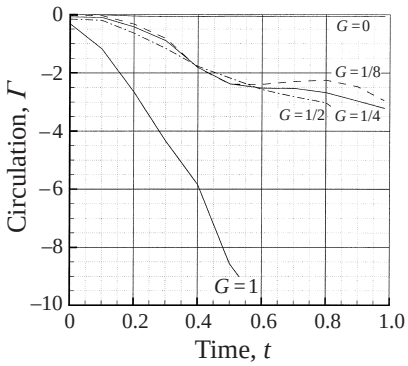

FIGURE 13. $Pe = 2000$, $R = 3$, $A = 0.5$, $G = 0$, 0.125, 0.25, 0.5, and 1: overall circulation in the flow field as a function of time. In general, the circulation grows both with time as well as with G, which indicates that eventually a gravity tongue will emerge, as long as the reservoir is long enough. However, as long as no gravity tongue has evolved yet, the curves for different values of G remain quite similar.

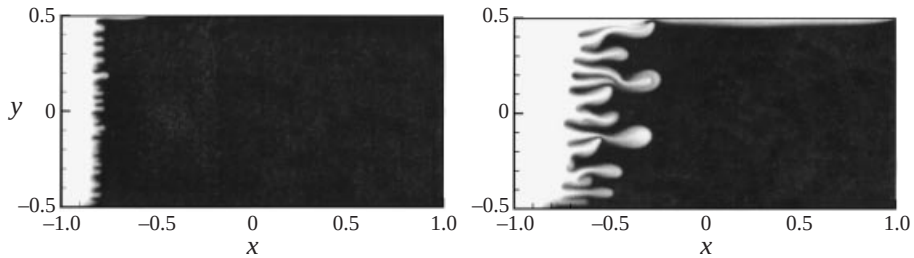

FIGURE 14. $Pe = 2000$, $G = 2$, $R = 3$, and $A = 0.5$: concentration field at times $t = 0.1$ and 0.387. At this high level of gravitational forces, a dominant gravity tongue quickly forms. Nevertheless, vigorous fingering still occurs across the entire displacement front.

conditions. Consequently, the gravity tongue is seen to develop more rapidly, cf. figures 14 and 15. Furthermore, it is seen to increase in thickness with time, in agreement with the findings of Tchelepi (1994). At the same time, the frontal sections near the bottom of the reservoir are slowed by the potential velocity, and they advance more slowly from the outset. In this way, the front gradually tilts and develops a globally inclined shape. At these large gravitational parameter values, the effect of the potential velocity component is no longer limited to the regions next to the upper and lower borders. Instead, it extends all the way into the central regions of the reservoir. Figure 7 shows that this potential velocity field has a free stagnation point near the centre of the reservoir, which contributes to the tilting of the mixed zone.

As the less-viscous fluid increasingly flows through the gravity tongue, the mean displacement velocity of the front in the remainder of the reservoir is reduced, thereby leading to a marked slowdown in the growth of the fingers. This is also reflected by the streamfunction plot (figure 16), whose equidistant contours indicate that a large fraction of the mass flux occurs near the top boundary. An increasing number of the finger tips can be seen to curve upward, at least in part due to the buoyancy forces they experience. This reflects a growing tendency towards the development of 'diagonal fingering' (Rogerson & Meiburg 1993*b*), i.e. the emergence of significant vertical velocities even within the fingering zone.

If gravitational effects increase further, the sections of the front below the gravity

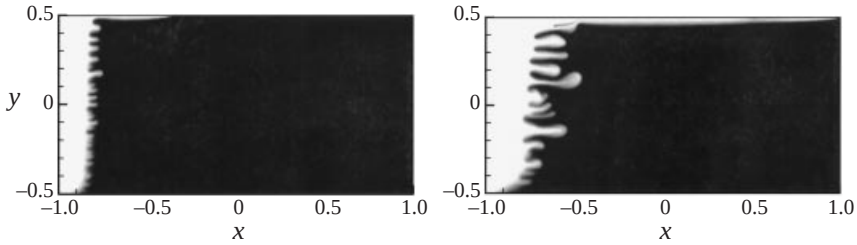

FIGURE 15. $Pe = 2000$, $G = 4$, $R = 3$, and $A = 0.5$: concentration field at times $t = 0.1$ and 0.270. As the lighter and less-viscous fluid increasingly flows through the gravity tongue, the fingering in the central regions of the domain slowly decreases in strength, due to the reduced effective displacement velocity.

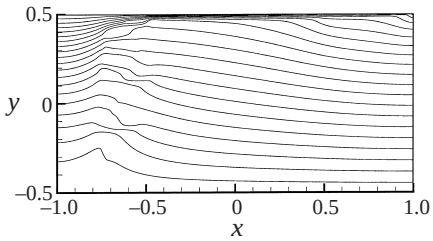

FIGURE 16. $Pe = 2000$, $G = 4$, $R = 3$, and $A = 0.5$: streamfunction contours at time $t = 0.270$. A relatively large fraction of the displacing fluid flows through the gravity tongue, thereby reducing the effective displacement velocity of the rest of the front.

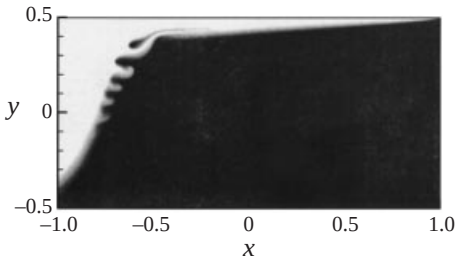

FIGURE 17. $Pe = 2000$, $G = 10$, $R = 2.5$, and $A = 0.5$: concentration field at time of breakthrough $t = 0.230$. Fingering below the gravity tongue is largely suppressed at this high value of G. Near the bottom boundary, there is an area of reverse flow.

tongue gradually stabilize due to the decreasing effective displacement velocity of these parts of the front, as well as to the shear stabilization mechanism described by Rogerson & Meiburg (1993*a*, *b*), cf. figure 17 for $Pe = 2000$, $G = 10$, $R = 2.5$, $A = 0.5$. The tilting of the front now proceeds so rapidly that a reverse flow occurs near the bottom of the reservoir, where the front propagates towards the injection well.

4.3. *Influence of viscosity parameter R*

The case $Pe = 2000$, $G = 1$, $R = 2$, and $A = 0.5$ illustrates the role of the viscosity contrast, cf. figure 18. When compared to the reference case shown in figure 2, the fingering during the earlier stages is seen to be somewhat less vigorous at this lower value of R, i.e. fewer fingers emerge, and they develop more slowly. Since both linear stability theory (Rogerson & Meiburg 1993*a*) as well as nonlinear simulations (Rogerson & Meiburg 1993*b*) for displacements perpendicular to the direction of gravity in

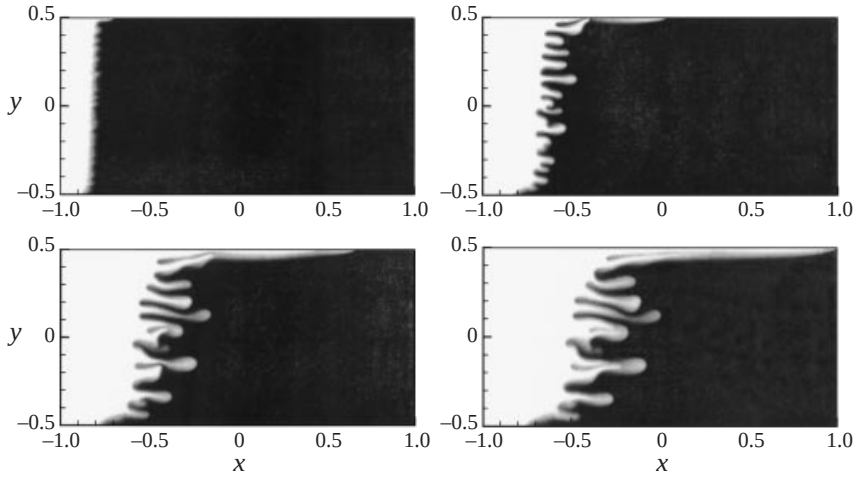

FIGURE 18. $Pe = 2000$, $G = 1$, $R = 2$, and $A = 0.5$: Concentration field at times $t = 0.1$, 0.3, 0.5, 0.613. While the fingering is less vigorous at this reduced viscosity contrast, the front develops an overall inclination more rapidly than for $R = 3$.

infinite domains, predict lower growth rates and larger instability wavelengths for reduced viscosity contrasts, this behaviour is in line with expectations. We furthermore notice that the gravity tongue is thicker, and that it proceeds somewhat more slowly for the lower value of R. This underlines that both size and propagation velocity of the gravity tongue are governed by similar mechanisms to the usual viscous fingering resulting from an instability. Interestingly, the global tilting of the mixed zone is more pronounced than for the case $R = 3$. The reason for this can be traced back to the vorticity equation (2.16). It states that the gravitational vorticity component, which drives the tilting of the front, is inversely proportional to the local viscosity value. Since the dimensionless viscosity varies between 1 and e^R, the integral over the gravitational vorticity component, i.e. the gravitational circulation, will be larger for $R = 2$ than for $R = 3$, as long as G remains unchanged. This is in contrast to the viscosity-related vorticity component, which grows with R. In summary, as R gets larger for constant G, we expect the fingering to increase in strength, but the angle of inclination of the mixed zone should grow more slowly.

The above line of reasoning is confirmed by the simulation of the case $Pe = 2000$, $G = 1$, $A = 0.5$, and $R = 0.25$, see figure 19. For this very small viscosity contrast, the entire interface tilts quite rapidly, while no fingering instability is observed.

4.4. *Influence of dimensionless flow rate Pe*

Figure 20 depicts the evolution of the flow for $Pe = 500$, $G = 1$, $R = 3$, and $A = 0.5$. Fewer and wider fingers emerge at this lower Pe-value in comparison to the reference case, and they grow more slowly. The pronounced gravity tongue developing along the top of the domain is wider than in the reference case as well, in line with the general trend that larger Pe-values result in a reduction of the dominant lateral length scale. This finding also agrees with earlier observations by Tchelepi (1994), who investigated the influence of the transverse Péclet number on the shape and propagation velocity of the gravity tongue. It is interesting to note that in the present simulations the gravity tongue, in spite of emerging later at $Pe = 500$, subsequently propagates at nearly the same velocity as for $Pe = 2000$. Since for $Pe = 500$ the fingers below the

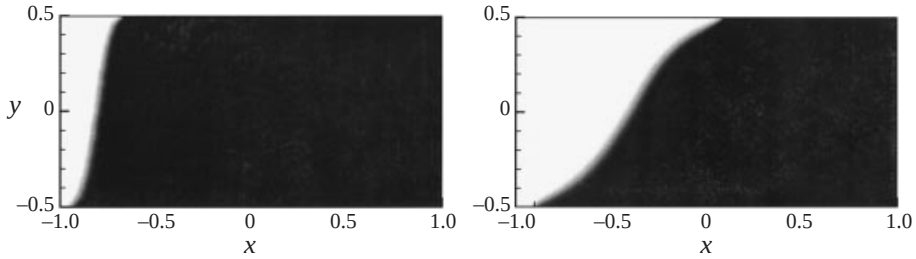

FIGURE 19. $Pe = 2000$, $G = 1$, $R = 0.25$, and $A = 0.5$: concentration field at times $t = 0.1$ and 0.5. At this very small value of R, no fingering occurs, but the global tilting of the front proceeds very quickly.

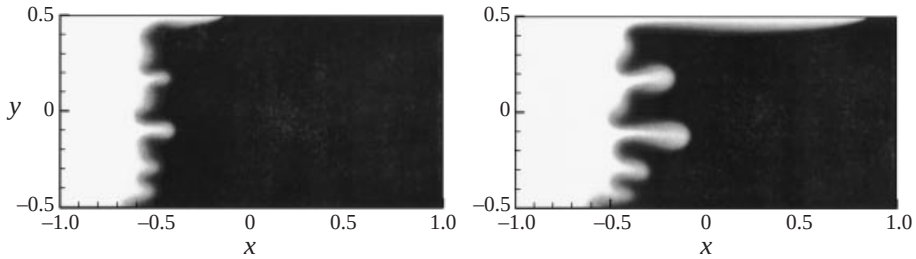

FIGURE 20. $Pe = 500$, $G = 1$, $A = 0.5$, and $R = 3$: concentration field at times $t = 0.3$ and 0.5. At this lower Pe-value, the fingers are thicker and spaced more widely apart. As a result, the dynamic interaction observed at $Pe = 2000$ between the gravity tongue and the finger immediately below it is absent here.

gravity tongue grow more slowly, and since they are also spaced more widely than for $Pe = 2000$, the interactions between the gravity tongue and the finger below it are absent at this smaller Pe-value, at least for the present value of the aspect ratio. The breakthrough occurs at nearly identical times for the two Pe-values. This behaviour indicates that, at least for $R = 3$, the breakthrough time does not depend strongly on the value of Pe, as long as a gravity tongue evolves.

An intermediate case is shown in figure 21 for $Pe = 1000$, $G = 1$, $R = 3$, and $A = 0.5$. While initially fewer fingers develop than in the reference case, some of the same interactions between the gravity tongue and the neighbouring finger can be observed. At later times, multiple mergers take place in the centre of the domain, so that very few large-scale fingers survive until the time of breakthrough.

4.5. *Influence of aspect ratio A*

Figure 22 shows the evolution of the displacement for $Pe = 500$, $G = 1$, $R = 3$, and $A = 0.125$. At time $t = 0.5$, the concentration field is still nearly identical to the case of $A = 0.5$ discussed above, for which breakthrough was observed shortly thereafter. This indicates that the downstream boundary of the domain does not have an appreciable effect on the dynamics of the fingering process until just before the leading finger reaches this boundary. This finding is in agreement with observations made by Tchelepi (1994). For $t \geqslant 0.8$, we observe interactions of the gravity tongue with the neighbouring finger that are quite similar to those described earlier for $Pe = 2000$. Pinching and partial merging events are clearly visible. This indicates that the same mechanisms are active at these lower Pe-values, but only after a longer time, so that they may manifest themselves only in smaller aspect ratio geometries.

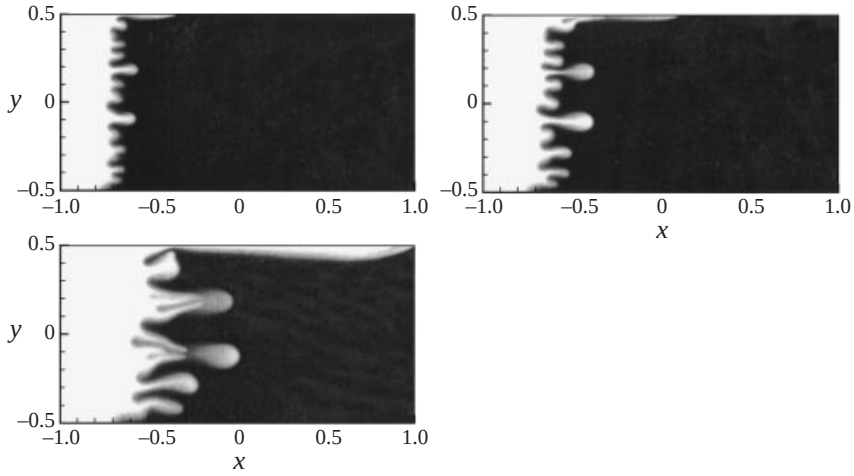

FIGURE 21. $Pe = 1000$, $G = 1$, $A = 0.5$, and $R = 3$: concentration field at times $t = 0.2, 0.3$, and 0.544. The gravity tongue strongly interacts with the finger next to it, while multiple mergers occur in the centre of the domain.

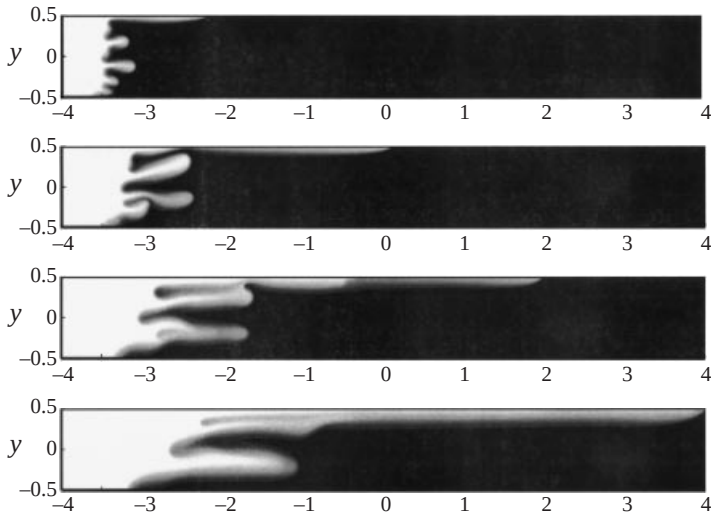

FIGURE 22. $Pe = 500$, $G = 1$, $A = 0.125$, and $R = 3$: concentration field at times $t = 0.5, 1, 1.6, 2.434$. In this longer domain, interactions between the gravity tongue and the finger below it occur that are similar to those observed for $A = 0.5$ and $Pe = 2000$.

Since this observation was also made for other parameter combinations, it suggests that the aspect ratio should enter into scaling arguments such as those proposed by Tchelepi (1994), even when diffusive or dispersive effects are present.

4.6. *Quantification of the global displacement features*

4.6.1. *Transversely averaged concentration profiles and mixing zone length*

For many practical applications involving porous media displacements, it is highly desirable to develop essentially one-dimensional models that are able to predict accurately the spatio-temporal evolution of the concentration profile averaged in the transverse direction. Towards this end, several researchers have investigated the

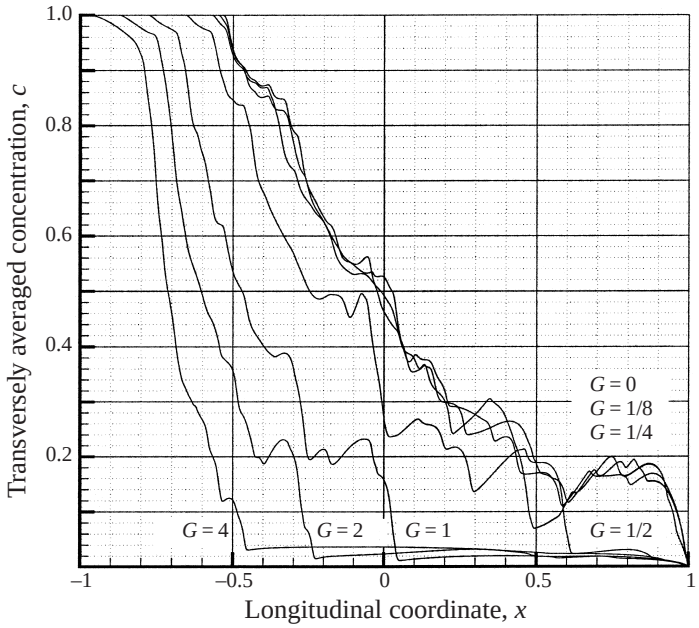

FIGURE 23. Transversely averaged concentration profiles for $Pe = 2000$, $R = 3$, $A = 0.5$, and $G = 0, 0.125, 0.25, 0.5, 1, 2$, and 4 at the time of breakthrough. In those flows that are dominated by a gravity tongue, the wiggly plateau known from neutrally buoyant displacements is preceded by another, much lower plateau that reflects the narrow gravity tongue.

properties of such averaged profiles as a function of the governing parameters. In the absence of density variations, Tan & Homsy (1988) found that for small initial perturbations, these transversely averaged concentration profiles at first evolve according to a one-dimensional convection–diffusion equation. During this phase the mixing length, defined as the distance between the locations where the averaged concentration profile takes the values of 0.1 and 0.9, respectively, grows proportionally to $t^{1/2}$. However, soon a plateau-like zone evolves that reflects the averaged properties of the fingering zone, and from then on the mixing length is observed to grow linearly with time. Interestingly, for large Pe the length of the mixing zone becomes nearly independent of Pe.

Figure 23 shows how the transversely averaged concentration profile at the time of breakthrough changes with G for $Pe = 2000$, $R = 3$, and $A = 0.5$. For $G = 0, 0.125$, and 0.25, the profiles look quite similar to those obtained by Tan & Homsy (1988), in that they display a wiggly, plateau-like region with values in the range 0.1 to 0.2, followed by a region of steep incline in which the value rises to 1. However, for $G = 0.5$ and 1, respectively, this plateau region is preceded by another, much lower region that reflects the existence of the gravity tongue. For the case $G = 0$ models have been derived that allow the prediction of the breakthrough time, cf. Tan & Homsy (1988) and references therein. However, for $G \neq 0$, such predictive models do not exist. In order to develop them, it is of interest to derive the relevant scaling laws that establish how this tongue's properties vary with the governing dimensionless parameters. In particular, we are interested in the thickness d of the tongue, which we consider to be given by the value of the concentration plateau when such a plateau exists. By measuring and comparing the tongue thickness for different G-values in simulations with constant R, Pe, and A, we found that $d \propto G^{1/2}$. In a similar fashion,

it was found that $d \propto Pe^{-1/2}$. For R, we did not observe such a uniformly valid law. While the thickness of the gravity tongue always decreased with increasing R, the exact quantitative dependence varied with G and Pe. The observed scaling

$$d \propto \left(\frac{G}{Pe}\right)^{1/2} \tag{4.7}$$

can be interpreted as follows (Homsy 2000). In dimensional quantities, it leads to

$$d \propto \left(\frac{V}{U}\right)^{1/2} \left(\frac{DH}{U}\right)^{1/2} \tag{4.8}$$

which suggests that the early formation of the tongue is governed by the ratio V/U, whereas its subsequent temporal evolution is dominated by diffusion. This interpretation is consistent with the above description of the two components of the potential velocity field, i.e. the uniform base flow and the constribution due to the horizontal boundaries. The strength of the focusing effect responsible for the formation of the gravity tongue is determined by the relative magnitude of these two components, i.e. by V/U.

4.6.2. *Breakthrough time*

For applications such as enhanced oil recovery, a crucial parameter is the breakthrough time, which we define as the time when the outflow boundary first sees a local concentration value of 0.5. It should be pointed out that there are also alternative definitions of breakthrough that take into account the averaged concentration at the outflow. Directly related to the breakthrough time is the recovery rate, which indicates the percentage of the displaced fluid pushed out of the domain by the time breakthrough occurs.

Figure 24 depicts the dependence of the recovery on G for different values of R, at $Pe = 2000$ and $A = 0.5$. For this relatively short reservoir, there is not sufficient time for a dominant gravity tongue to develop for small values of G. As a result, there is a small plateau-like region near $G = 0$, for which the breakthrough recovery does not depend on G. Interestingly, the size of this plateau region depends on the value of R. For $G = 0.25$, the $R = 2$ case develops a gravity tongue and consequently breaks through *earlier* than the $R = 2.5$ flow, for which a gravity tongue does not form. This indicates a dependence on R of the G-value at which the transition from fingering-dominated to gravity-dominated flow occurs, in line with observations by Tchelepi (1994).

For larger values of G, however, the recovery quickly drops, due to the rapid formation of a dominant gravity tongue that results in earlier breakthrough. Interestingly, over the fairly large range of G-values investigated here, an increase in R from 2 to 3 cuts the recovery by approximately the same number of percentage points. The same behavior is observed for $Pe = 500$, cf. figure 25.

4.6.3. *Growth of interfacial length*

In many practical applications, important mechanisms such as, for example, chemical reactions (De Wit & Homsy 1999) are active in the interfacial region of the flow field where the two phases are in contact with each other. As a result, it is of interest to track the growth of this interfacial area. Strictly speaking, of course, a sharp interface does not exist between two miscible fluids. However, Chen & Meiburg (1998*a*) showed that the evolution of the interfacial length $l(t)$ in a two-dimensional

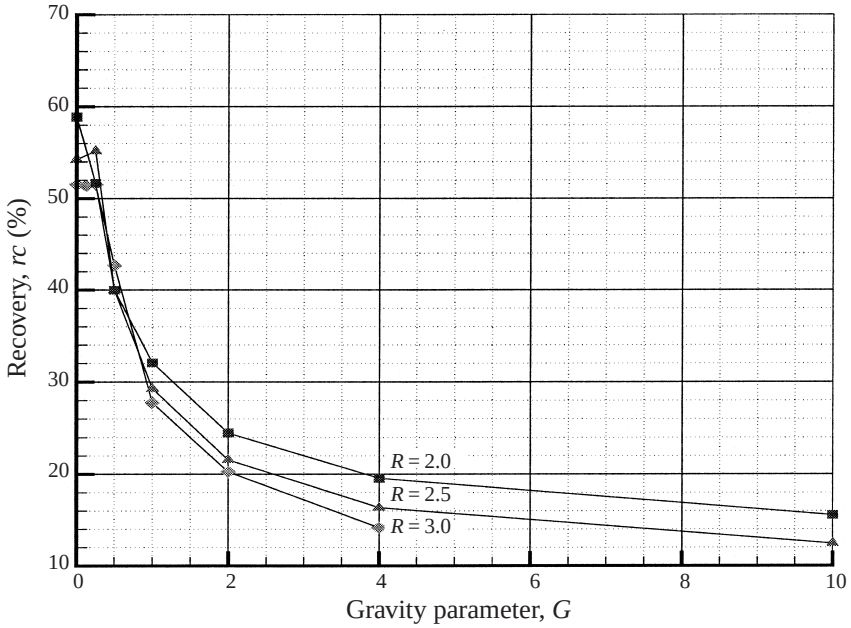

FIGURE 24. Dependence of the breakthrough recovery on G for different values of R, at $Pe = 2000$ and $A = 0.5$. For values of G sufficiently small that a dominant gravity tongue does not form before breakthrough, a plateau-like region exists in which the breakthrough recovery is largely independent of G. For larger values of G, the recovery quickly drops.

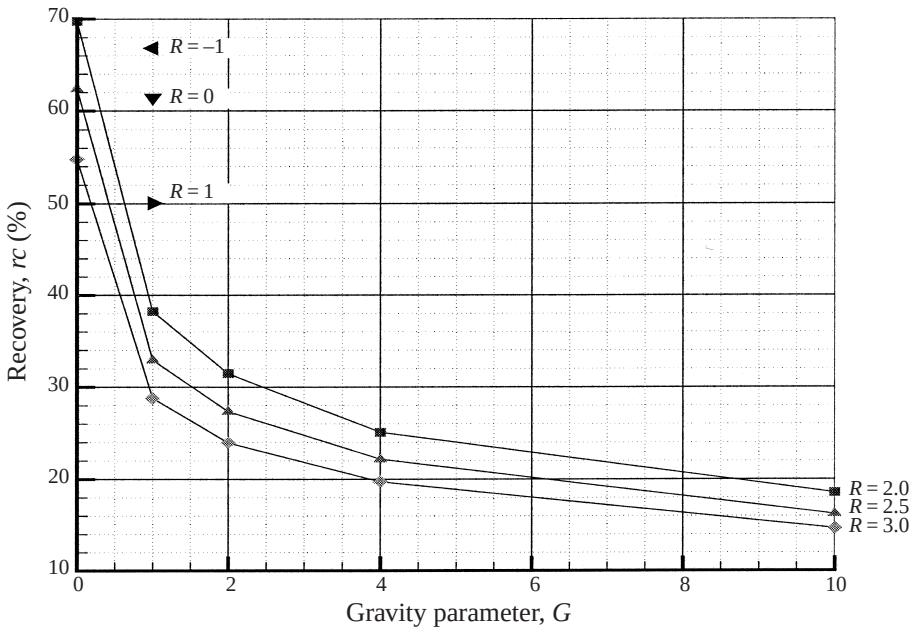

FIGURE 25. Dependence of the breakthrough recovery on G for different values of R, at $Pe = 500$ and $A = 0.5$. While the overall behaviour is similar to the data for $Pe = 2000$, the plateau regions for small G are not observed.

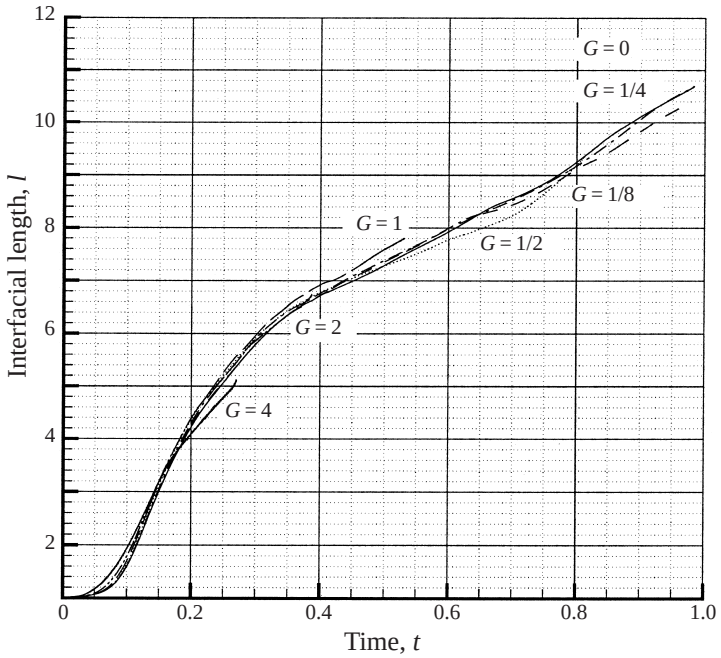

FIGURE 26. Interfacial growth for $Pe = 2000$, $R = 3$, $A = 0.5$, and $G = 0, 0.125, 0.25, 0.5, 1, 2$, and 4. For these moderate values of G, the growth of $l(t)$ is nearly independent of G.

flow can be monitored as

$$l = \int_S \left(c_x^2 + c_y^2\right)^{1/2} \mathrm{d}S. \tag{4.9}$$

For the case of a stably propagating front, $l = 1$ for all times. For $Pe = 2000$ and $A = 0.5$, figure 26 depicts the interfacial growth for $R = 3$ and $G = 0, 0.125, 0.25, 0.5, 1, 2$, and 4.

Interestingly, for these large Pe-values and moderate values of G, the growth of $l(t)$ is largely independent of G, since in all cases a vigorous fingering activity develops. However, further simulations for other parameter combinations show that at very large G-values the rapid growth of the gravity tongue cannot make up for the loss of interfacial growth due to the reduced fingering, so that the overall growth of $l(t)$ slows down markedly.

4.6.4. *Global tilting of the mixed region*

It is desirable to quantify the overall 'tilt' of the mixed region due to the density differences. Towards this end, we compare the actual concentration field $c(x, y, t)$ with the one-dimensional reference field $c_0(x, t)$ that would be obtained at the same time for a stably propagating front in the absence of density differences and diffusion. This reference profile thus has the same thickness as the actual profile at the beginning of the simulation. We can then define the quantity $\Omega(t)$

$$\Omega = \int_S \beta(y)\ [c(x, y, t) - c_0(x, t)]\ \mathrm{d}S, \tag{4.10}$$

where

$$y > 0: \quad \beta = 1, \tag{4.11a}$$

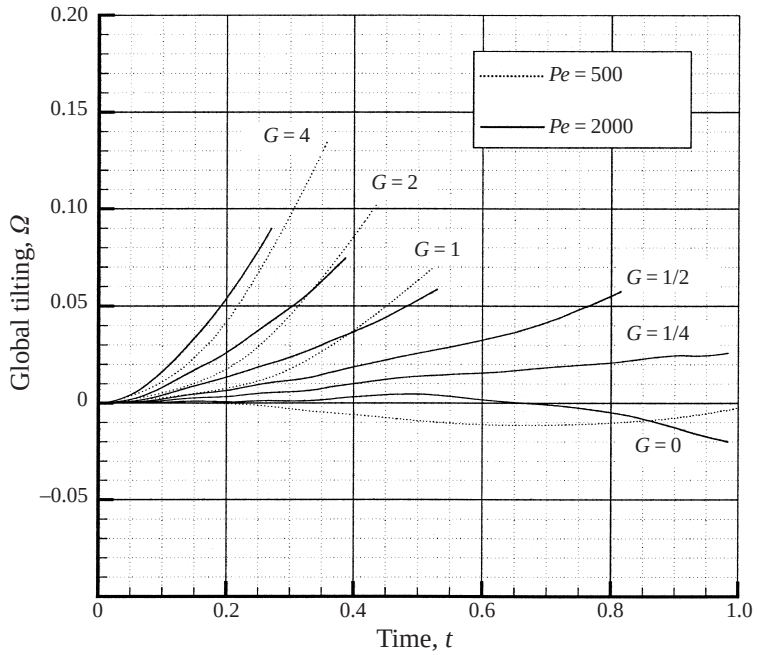

FIGURE 27. Global tilting $\Omega(t)$ for $R = 3$, $A = 0.5$, $Pe = 500$ and 2000, and various values of G. For constant Pe-values, during the early stages $\Omega \propto G$.

$$y < 0: \quad \beta = -1. \tag{4.11b}$$

A value of Ω larger (smaller) than zero indicates a global tilting of the interfacial region in the clockwise (counterclockwise) direction.

Figure 27 indicates that, approximately, $\Omega \propto G$ during the early stages. Very early on, $\Omega(t)$ is seen to grow more rapidly for larger Pe, which reflects the faster formation of a gravity tongue. For longer times, however, smaller Pe display larger Ω-values, as a result of the increased thickness of the tongue at lower Pe.

Figure 28 displays the dependence of $\Omega(t)$ on R. For positive R-values, the graphs confirm our earlier qualitative observation that global tilting proceeds more slowly with increasing R, since the gravitational circulation is reduced. For comparison, we also include a stable case $R = -1$. In this case, the density field promotes global tilting, whereas the viscosity field favours a straight vertical interface. After an initial transient, the competition between the two effects leads to a reduced tilting rate.

4.6.5. *Rate of propagation of finger tip*

Figure 29 shows the tip location of the most advanced finger, defined as the largest x-location with a concentration value above 0.5, as a function of time for a variety of parameter combinations and $Pe = 2000$. The results for $G = 0$ confirm earlier findings for flows without density differences (cf. Tan & Homsy 1988; Tchelepi 1994) by showing that after an initial transient the most advanced finger propagates with a constant velocity that increases with R. This behaviour does not persist in the presence of density differences that are sufficiently strong to result in the emergence of a gravity tongue. Here, after an initial transient acceleration phase, the gravity tongue reaches a maximum velocity. Subsequently, it is seen to slow down somewhat, but a renewed acceleration can occur as well. This reflects the time-dependent variations in

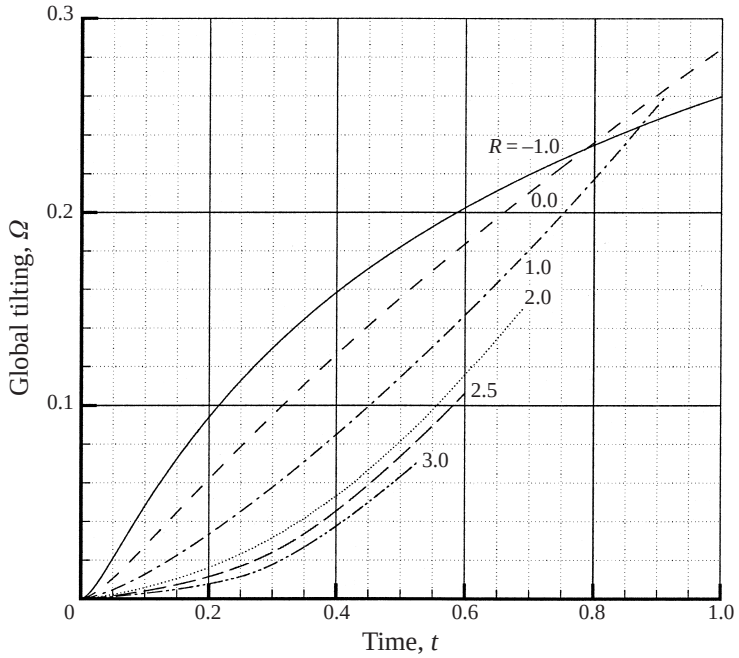

FIGURE 28. Global tilting $\Omega(t)$ for $Pe = 500$, $A = 0.5$, $G = 1$, and various R-values. For positive values of R, the tilting rate decreases with increasing R.

the supply of less-viscous fluid to the gravity tongue, as had been observed to occur for some parameter combinations. These variations affect the unfavourable viscosity gradient at the tip of the tongue and cause it to fluctuate with time. Both pinching by the neighbouring finger as well as lateral diffusion along the length of the tongue can reduce this supply, while a partial merger with the neighbouring finger can replenish it. The sudden jump seen in the graph for $G = 1$ and $R = 3$ results from such a pinching event, which caused the maximum concentration at the tip of the gravity tongue to drop below the value of 0.5. However, the long-term propagation rate of the finger tip approaches a constant value again. This finding again is in agreement with observations by Tchelepi (1994).

An interesting phenomenon can be observed during the initial transient acceleration phase, cf. figure 30, which represents a detail of figure 29. It can be seen that for $G = 1$ the gravity tongue in the $R = 2$ displacement initially accelerates more rapidly than for larger R-values. While this behaviour is reversed later, it is nevertheless noteworthy, since it is in contrast to observations for the growth of the most advanced finger when $G = 0$. The key to understanding this behaviour again lies in the vorticity equation (2.16). At early times, when the front is still approximately one-dimensional, the viscosity-related vorticity component is still quite small, since both c_y and v are small. The gravity-related vorticity component, on the other hand, is strong from the very beginning. However, the larger R is, the larger μ will be on average across the front. Since μ appears in the denominator of the gravity-related vorticity, the latter will be larger for *smaller* R, i.e. the overall tilting due to gravity will proceed more quickly. Soon, however, this leads to deviations in the overall frontal shape, so that eventually the viscosity-related vorticity will take over.

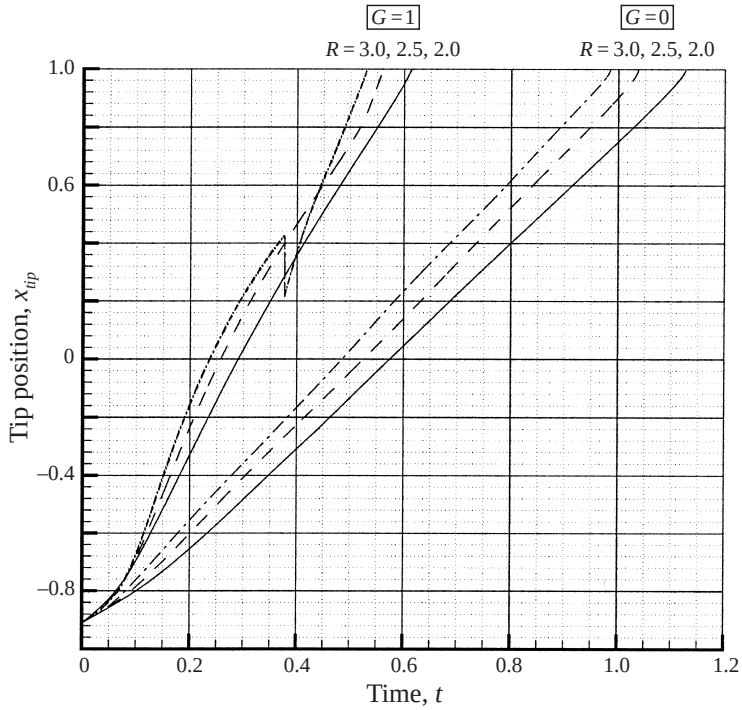

FIGURE 29. Tip location of the most advanced finger as function of G and R for $Pe = 2000$ and $A = 0.5$. In contrast to neutrally buoyant displacements, the tip velocity in flows dominated by a gravity tongue usually does not approach a constant value. This is due to variations in the supply of less-viscous fluid to the tip of the gravity tongue

5. Conclusions

The focus of the present investigation is on analysing the dynamics of rectilinear, homogeneous miscible displacements with gravity override on the basis of the vorticity–streamfunction formulation of the governing equations. While a number of the observed flow features had previously been reported, the vorticity-based point of view often allows one to attribute these flow characteristics more clearly to the effects of viscosity differences, density differences, or impermeable boundaries. In particular, it enables us to understand the formation of the gravity tongue in terms of a focusing mechanism. This focusing mechanism is generated by the potential flow field, which consists of two separate contributions. Superimposed on the time-independent uniform base flow is the potential flow component generated by the horizontal boundaries at the top and bottom of the reservoir, which enforce the condition of vanishing normal flow. This component of the potential flow field evolves with the flow, and it is approximately proportional to the gravitational rise velocity. The overall potential flow field has a streamwise velocity maximum near the upper wall, which in conjunction with the unfavourable viscosity gradient leads to strong local growth of a viscous fingering instability. This strong local growth, in turn, manifests itself in kthe form of a rapidly growing gravity tongue. In this way, the emergence of the gravity tongue can be attributed to a local enhancement of the same basic instability mechanism that is active across the entire interface. The numerical simulations for different values of the governing parameters lead to scaling results which demonstrate that the thickness of the gravity tongue grows with $(G/Pe)^{1/2}$. This result indicates that the intial formation

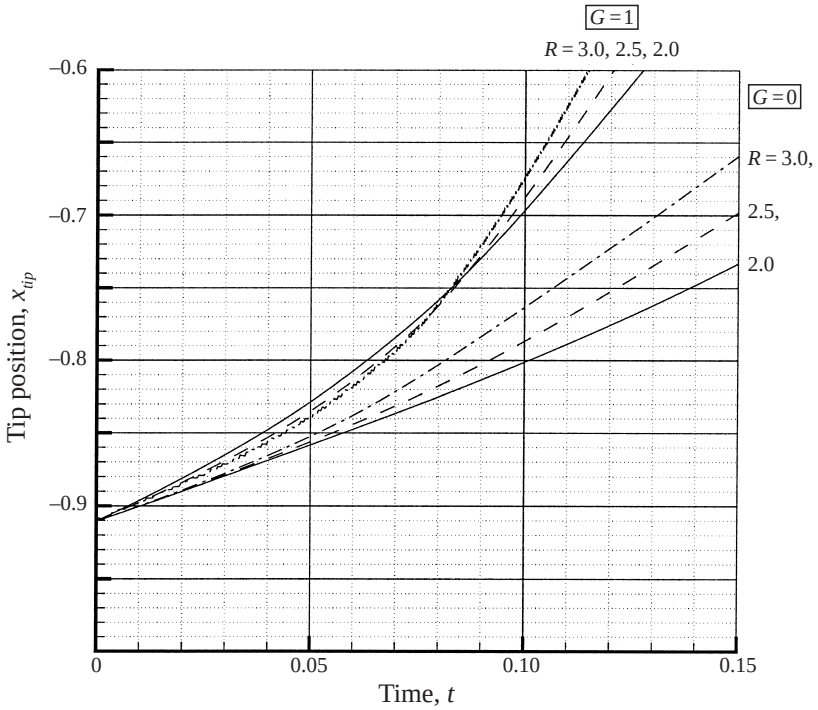

FIGURE 30. Detail of figure 29 for short times. Initially, the front can propagate more rapidly for smaller R-values.

of the gravity tongue is related to the relative strengths of the two components of the potential velocity field, while its subsequent change in thickness is governed by diffusive effects. When interpreting the present, two-dimensional results, it is to be kept in mind that the relative strengths of viscously driven and gravitationallly driven effects can change in three dimensions, so that there is a strong motivation for us to extend the present investigation to include a third dimension.

Another interesting extension concerns the inclusion of permeability heterogeneities. In particular, the role of the resonance mechanism observed for neutrally buoyant flows (Tan & Homsy 1992; De Wit & Homsy 1997*a*, *b*; Chen & Meiburg 1998*b*) will have to be investigated in detail in the presence of density differences. This will require a careful study of the interactions among all three of the vorticity components, as well as the potential velocity field, which will be the subject of Part 2 of the present investigation.

The authors would like to acknowledge helpful discussions with Dr Hamdi Tchelepi and Professor G. M. Homsy. This research is supported by the donors of The Petroleum Research Fund, administered by the American Chemical Society (Grant ACS-PRF No. 33497-AC9), and by the Chevron Petroleum Technology Company. The simulations were partially carried out at the San Diego Supercomputer Center, which is funded by the National Science Foundation.

REFERENCES

ARAKTINGI, U. G. & ORR, F. M. 1993 Viscous fingering in heterogeneous porous media. *SPE Advanced Technology Series* **1**(1), pp. 71–80.

Bacri, J.-C., Rakotomalala, N., Salin, D. & Woumeni 1992 Miscible viscous fingering: Experiments versus continuum approach. *Phys. Fluids* A **4**, 1611–1619.

Batycky, R. P., Blunt, M. J. & Thiele, M. R. 1996 A 3D field scale streamline simulator with gravity and changing well conditions. *SPE Paper* 36726.

Blackwell, R. J., Rayne, J. R. & Terry, W. M. 1959 Factors influencing the efficiency of miscible displacement. *Trans. AIME* **216**, 1–8.

Brady, J. F. & Koch, D. L. 1988 In *Disorder and Mixing* (ed. E. Guyon *et al.*). NATO ASI Series E. Academic.

Camhi, E., Meiburg, E. & Ruith, M. 1999 Miscible rectilinear displacements with gravity override. Part 2. Heterogeneous porous media. *J. Fluid Mech.* **420**, 259–276.

Canuto, C., Hussaini, M. Y., Quarteroni, A. & Zang, T. A. 1988 *Spectral Methods in Fluid Mechanics.* Springer.

Chang, Y.-B., Lim, M. T., Pope, G. A. & Sepehrnoori, K. 1991 Carbon dioxide flow patterns under multiphase flow, heterogenous field scale conditions. *SPE Paper* 22654, presented at the 1991 SPE Annual Technical Conference and Exhibition, Dallas, TX, October 6–9.

Chen, C.-Y. 1998 Topics in miscible porous media flows. PhD dissertation, University of Southern California, Los Angeles, California.

Chen, C.-Y. & Meiburg, E. 1996 Miscible displacements in a capillary tube. Part 2. Numerical simulations. *J. Fluid Mech.* **326**, 57–90.

Chen, C.-Y. & Meiburg, E. 1998*a* Miscible porous media displacements in the quarter five-spot configuration. Part 1. The homogeneous case. *J. Fluid Mech.* **371**, 233–268.

Chen, C.-Y. & Meiburg, E. 1998*b* Miscible porous media displacements in the quarter five-spot configuration. Part 2. Effect of heterogeneities. *J. Fluid Mech.* **371**, 269–299.

Christie, M. A., Jones, A. D. W. & Muggeridge, A. H. 1990 Comparison between laboratory experiments and detailed simulations of unstable miscible displacement influenced by gravity. In *North Sea Oil and Gas Reservoirs II* (ed. A. T. Buller *et al.*). Graham and Trotman, London.

Christie, M. A., Muggeridge, A. H. & Barley, J. J. 1993 3D simulation of viscous fingering and WAG schemes. *SPE Res. Engng* **8**, 19–26.

Crane, F. E., Kendall, H. A. & Gardner, G. H. F. 1963 Some experiments on the flow of miscible fluids of unequal density through porous media. *Soc. Petrol. Engrs J.*, 277–280.

de Wit, A. & Homsy, G. M. 1997*a* Viscous fingering in periodically heterogeneous porous media. I. Formulation and linear instability. *J. Chem. Phys.* **107**, 9609–9618.

de Wit, A. & Homsy, G. M. 1997*b* Viscous fingering in periodically heterogeneous porous media. I. Numerical simulations. *J. Chem. Phys.* **107**, 9619–9628.

de Wit, A. & Homsy, G. M. 1999 Nonlinear interactions of chemical reactions and viscous fingering in porous media. *Phys. Fluids* **11**, 949–954.

Dietz, D. N. 1953 A theoretical approach to the problem of encroaching and bypassing edge water. *Proc. Koninkl. Ned. Akad. Wetenschap* **B56**, 83–92.

Fayers, F. J. & Muggeridge, A. H. 1990 Extensions to Dietz theory and behavior of gravity tongues in slightly tilted reservoirs. *SPE Res. Engng* **5**, 487–494.

Gorell, S. 1992 Outlook for calibration of large grid-block models for miscible flooding applications. *SPE Paper* 24186, presented at the 1992 SPE/DOE Eighth Symposium on Enhanced Oil Recovery. Tulsa, OK, April.

Gottlieb, D. & Orszag, S. A. 1977 *Numerical Analysis of Spectral Methods: Theory and Applications.* SIAM.

Hill, S. 1952 Channelling in packed columns. *Chem. Engng Sci.* **1**.

Homsy, G. M. 1987 Viscous fingering in porous media. *Ann. Rev. Fluid Mech.* **19**, 271–311.

Horne, R. N. & Rodriguez, F. 1983 Dispersion in tracer flow in fractured geothermal systems. *Geophys. Res. Lett.* **10**, 289.

Josselin de Jong, de 1960 Singularity distributions for the analysis of multiple-fluid flow through porous media. *J. Geophys. Res.* **65**, 3739–3758.

Lele, S. K. 1992 Compact finite difference schemes with spectral-like resolution. *J. Comput. Phys.* **103**, 16–42.

Manickam, O. & Homsy, G. M. 1993 Stability of miscible displacements in porous media with nonmonotonic viscosity profiles. *Phys. Fluids* A **5**, 1356–1367.

Manickam, O. & Homsy, G. M. 1994 Simulation of viscous fingering in miscible displacements with nonmonotonic viscosity profiles. *Phys. Fluids* **6**, 95–107.

McCloud, K. V. & Maher, J. V. 1995 Experimental perturbations to Saffman-Taylor flow. *Phys. Rep.* **260**, 139–185.

Meiburg, E. & Chen, C.-Y. 1998 High-accuracy implicit finite difference simulations of homogeneous and heterogeneous miscible porous media flows. *Soc. Petrol. Engrs J.* **5**(2), 129–137.

Meiburg, E. & Homsy, G. M. 1988*a* Nonlinear unstable viscous fingers in Hele-Shaw flows. II. Numerical simulation. *Phys. Fluids* **31**, 429–439.

Meiburg, E. & Homsy, G. M. 1988*b* Vortex methods for porous media flows. In *Numerical Simulation in Oil Recovery* (ed. M. F. Wheeler). IMA Volumes in Mathematics and Its Applications 11, Springer.

Moisses, D. E., Miller, C. A. & Wheeler, M. F. 1989 Simulation of miscible viscous fingering using a modified method of characteristics: effects of gravity and heterogeneity. *SPE Paper* 18440, presented at the 1989 Tenth Symposium on Reservoir Simulation, Housten, TX, February.

Pankiewitz, C. & Meiburg, E. 1999 Miscible porous media displacements in the quarter five-spot configuration. Part 3. Non-monotonic viscosity profiles. *J. Fluid Mech.* **388**, 171–195.

Petitjeans, P., Chen, C.-Y., Meiburg, E. & Maxworthy, T. 1999 Miscible quarter five-spot displacements in a Hele-Shaw cell and the role of flow-induced dispersion. *Phys. Fluids* **11**, 1705–1716.

Petitjeans, P. & Maxworthy, T. 1996 Miscible displacements in a capillary tube. Part 1. Experiments. *J. Fluid Mech.* **326**, 37–56.

Pozzi, A. L. & Blackwell, R. J. 1963 Design of laboratory models for study of miscible displacement. *Soc. Petrol. Engng J.*, 28–40.

Rakotomalala, N., Salin, D. & Watzky, P. 1997 Miscible displacement between two parallel plates: BGK Lattice gas simulations. *J. Fluid Mech.* **338**, 277–297.

Rogerson, A. & Meiburg, E. 1993*a* Shear stabilization of miscible displacement process in porous media. *Phys. Fluids* A **5**, 2644–2660.

Rogerson, A. & Meiburg, E. 1993*b* Numerical simulation of miscible displacement processes in porous media flows under gravity. *Phys. Fluids* A **5**, 1344–1355.

Sheldon, J. W. & Fayers, F. J. 1962 The motion of an interface between two fluids in a slightly dipping reservoir. *Soc. Petrol. Engrs J.*, 275–282.

Sorbie, K. S., Feghi, F., Pickup, G. E., Ringrose, P. S. & Jensen, J. L. 1992 Flow regimes in miscible displacement in heterogeneous correlated random fields. *SPE Paper* 24140, presented at the 1992 SPE/DOE Eighth Symposium on Enhanced Oil Recovery. Tulsa, OK, April.

Sorbie, K. S., Zhang, H. R. & Tsibuklis, N. B. 1995 Linear viscous fingering: New experimental results, direct simulation and the evaluation of averaged models. *Chem. Engng Sci.* **50**, 601–616.

Tan, C. T. & Homsy, G. M. 1988 Simulation of nonlinear fingering in miscible displacement. *Phys. Fluids* **31**(6), 1330–1338.

Tan, C. T. & Homsy, G. M. 1992 Viscous fingering with permeability heterogeneity. *Phys. Fluids* A **4**, 1099–1101.

Taylor, G. I. 1953 Dispersion of soluble matter in solvent flowing slowly through a tube. *Proc. R. Soc. Lond.* A **219**, 186–203.

Tchelepi, H. A. 1994 Viscous fingering, gravity segregation and permeability heterogeneity in two-dimensional and three-dimensional flows. Dissertation, Department of Petroleum Engineering, School of Earth Sciences, Stanford University.

Tchelepi, H. A., Orr, F. M., Rakotomalala, N., Salin, D. & Woumeni, R. 1993 Dispersion, permeability heterogeneity, and viscous fingering: Acoustic experimental observations and particle-tracking simulations. *Phys. Fluids* A **5**, 1558–1574.

Tryggvason, G. & Aref, H. 1983 Numerical experiments on Hele-Shaw flow with a sharp interface. *J. Fluid Mech.* **136**, 1–30.

Tryggvason, G. & AREF, H. 1985 Finger interaction mechanism in stratified Hele-Shaw flow. *J. Fluid Mech.* **154**, 287–301.

Poel, C. van der 1962 Effect of lateral diffusivity on miscible displacement in horizontal reservoirs. *Soc. Petrol. Engrs J.*, 317–326.

Verruijt, A. 1980 The rotation of a vertical interface in a porous medium. *Wat. Resour. Res.* **16**, 239–240.

Waggoner, J. R., Castillo, J. L. & Lake, L. W. 1992 Simulation of EOR processes in stochastically generated permeable media. *SPE Formation Eval.*, 173–180.

Withjack, E. M. & Akervoll, I. 1988 Computed tomography studies of 3-D miscible displacement

behavior in a laboratory five-Spot model. *SPE Paper* 18096, presented at the 1988 SPE Annual Technical Conference and Exhibition, Houston, TX, October 2–5.

Wray, A. A. 1991 Minimal storage time-advancement schemes for spectral methods. Preprint.

Yang, Z. & Yortsos, Y. C. 1997 Asymptotic solutions of miscible displacements in geometries of large aspect ratio. *Phys. Fluids* **9**, 286.

Yortsos, Y. C. 1990 Instabilities in displacement processes in porous media. *J. Phys. Condens. Matter* **2**, SA443–SA448.

Yortsos, Y. C. & Zeybek, M. 1988 Dispersion driven instability in miscible displacement in porous media. *Phys. Fluids* **31**, 3511–3518.

Zhang, H. R., Sorbie, K. S. & Tsibuklis, N. B. 1997 Viscous fingering in five-spot experimental porous media: New experimental results and numerical simulation. *Chem. Engng Sci.* **52**, 37.

Zimmerman, W. B. & Homsy, G. M. 1991 Viscous fingering in miscible displacement with anisotropic dispersion. *Phys. Fluids* A **3**, 1859–1872.

Zimmerman, W. B. & Homsy, G. M. 1992 Three-dimensional viscous fingering: A numerical study. *Phys. Fluids* A **4**, 1901–1914.